University of Alberta

MECHANICAL PROPERTIES OF BIO- AND NANO-FILAMENTS

by

Abdorreza Samarbakhsh

A thesis submitted to the Faculty of Graduate Studies and Research
in partial fulfillment of the requirements for the degree of

Doctor of Philosophy

Department of Physics

Fall 2010
Edmonton, Alberta

Examining Committee

Jack Tuszynski, Physics and Oncology

Richard Marchand, Physics

Richard Sydora, Physics

Chong-Qing Ru, Mechanical Engineering

David Boal, Physics, Simon Fraser University

To

My wife, Neda
My parents, Shokrollah and Fatemeh
My sisters, Ladan, Leila, Laleh, and Nastaran

ABSTRACT

The thesis is divided in three parts based largely on published articles or on manuscripts submitted for publication. First we propose a new method which is called the shooting-bead method. This method is a fast and easy experimental technique for evaluating cantilever stiffness and flexural rigidity of semi-flexible to semi-rigid rod-like biological and nano-filaments based on the measurement of just two distances. The method is based on applying a force normal to the filament with a microsphere bead trapped in the laser tweezer followed by its sudden release. Through a simple measurement of the distances that the bead moves, the flexural rigidity of the filament can be found from the formula derived in this paper. Then we take into account the effects of the viscous drag force exerted on the filament itself. To this end, we have defined a key variable, called the filament energy-loss factor (or filament drag factor) that accounts for all the energy-loss effects. It has been shown that the effect due to the consideration of filament energy-loss factor on calculation of the flexural rigidity increases with increasing the flexibility of the filament. Finally, in the third part we discuss the effect of ultrasound on the microtubules. Here we have analytically solved equations of motion for the vibrational dynamics of an MT that is attached at its two ends. This is especially relevant for MTs during mitosis when they attach to chromosomes and centrosomes. Our analysis applies to MTs present inside a viscous solution and when driven by an ultrasound plane wave. We have shown that with using

ultrasound plane waves the resonance condition for the MT treated as a rigid rod cannot be provided, and in order to achieve resonance we should excite a single mode of the MT with a harmonic number larger than a threshold value introduced in this thesis. Single mode excitation not only helps to transfer the minimum amount of energy to the surrounding medium compared with multi-mode excitation but it also allows for a simultaneous high-amplitude and high-quality factor which is impossible when using plane waves.

ACKNOWLEDGMENTS

I would like to express my sincere thanks to my supervisor, Dr. Jack A. Tuszynski. He has been very helpful and provided me with constant supervision throughout my PhD at U of A. I would also like to thank him for his confidence in my work that granted me the professional freedom needed for creative production of original scientific work.

My special thanks go to Dr. Neda Naseri who has always assisted me with her superior computer skills and to Laleh Samarbakhsh for suggestions and comments on writing.

The theoretical design in the first part of this thesis further strengthened from the actual experiments on cytoskeleton filaments in the Cross Cancer Institute at U of A. I'd like to thank Dr. Linda Payet for agreeing to perform the preliminary tests.

I would like to thank Dr. David Boal, Dr. Richard Marchand, Dr. Chong-Qing Ru, and Dr. Richard Sydora for serving on my thesis committee. I have always enjoyed and learnt from the broad physics discussions with Dr. Richard Marchand during my sudies at U of A.

This is my humble opportunity to thank all physics professors and pioneers of this beautiful science who graciously authored textbooks with great flow and writing quality that can be self-studied. I am especially in debt to the following authors for the basics of my physics knowledge come from deep study of their invaluable textbooks:
W. Byron (with R. W. Fuller), H. Goldstein, D. J. Griffiths, D. Halliday (with R. Resnick), J. D. Jackson, J. B. Marion, M. H. Nayfeh (with M. K. Brussel), J. R. Reitz (with F. J. Milford and R. W. Christy), R. K. Pathria, J. J. Sakurai, R. Shankar, and S. Wieder,

Last but not least, I would like to thank my family and friends for their never-ending emotional support which is essential for my work. I love you.

Contents

List of Figures

Chapter 1

Introduction

In this introduction we aim to review two subjects. First we will briefly introduce the cytoskeleton, which is comprised of filamentous proteins that extend throughout the cytoplasm. Second, which most of this chapter is devoted to, we will summarize the related physics for the interested reader which is needed for clear understanding of this thesis.

1.1 Cytoskeleton

Eukaryotic cells contain three major classes of cytoskeletal filaments: actin filaments, intermediate filaments, and microtubules. They are made of either actin or tubulin or various structural proteins such as keratin. Each of these proteins actually defines a large family of structurally related proteins.

1.1.1 Actin Filaments

Actin filaments which are also called microfilaments, have a cable-like shape. Their diameters are about 6 nm. The building block of actin filaments is the actin monomer. The structure of an actin filament can be considered as either single-stranded or double-stranded. In the single-stranded consideration, it is a one-start, left-handed helix of actin monomers [1]. The full period of filaments is 72 nm which contains 26 subunits. Therefore, the rise is about 2.77 nm [2](Figure 1.1). As the rotation per monomer is large (166^o), and because there is extensive monomer-monomer contact between alternate monomers, the actin filament is more appropriately viewed as a two-stranded filament. In this case, it is a two-start, right-handed helix, with the strands, called protofilaments, half staggered and wrapping slowing round each other with a repeat period of 72 nm.

1.1.2 Microtubules

Microtubules, Figure 1.2, are the cytoskeleton's largest filaments. They are hollow cylinders which are formed from 13 protofilaments (from 8 to 19 protofilaments have been also reported [5]) aligned in parallel. Lateral and longitudinal interactions between the tubulin subunits are responsible for maintaining the tubular form. In the case of 13 protofilaments, which is the most common case for cellular microtubules [6], the outer diameter and inner diameter are 25 nm and 15 nm, respectively. The subunit of each protofilament is a tubulin heterodimer, formed from a very tightly linked pair of α- and

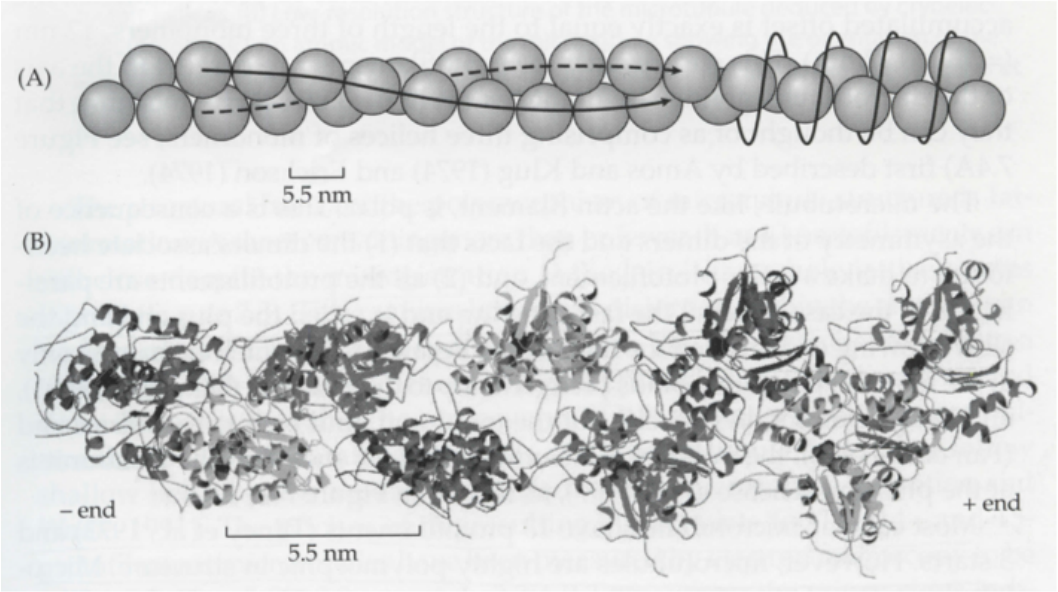

Figure 1.1 (A) Lattice structure showing the two-stranded (or two starts) representation on the left and the one-stranded representation on the right, courtesy of Jonathan Howard [3]. (B) The atomic model of the actin filament, courtesy of Geeves and Holmes [4].

β-tubulin monomers. They are joined end-to-end with alternating α- and β-tubulin monomers to form the protofilament. Each subunit is about 8 nm long, 5 nm wide, and 5 nm thick. If we consider the position of each subunit in the microtubule, due to the organised positioning of subunits, we can represent the microtubule as a regular lattice. Microtubules have been observed in two forms of lattices which are called the A-lattice and B-lattice, respectively. The structure of a B-lattice with 13 protofilaments is a perfect 3-start helix [6].

Microtubules play a key role in many important cellular activities. They are responsible for the beating of cilia and flagella, transportation of membrane vesicles in the cytoplasm, determination of cell shape and motility, organization and positioning of membrane organelles, and alignment and separation of chromosomes during mitosis. But the most critical role of MTs is to provide the mechanical force required for chromosome separation during mitosis. All the above movements result from the polymerization and de-polymerization of MTs or by the action of molecular motor proteins along microtubules. Also due to the central role of microtubules in mitosis, anything that affects microtubule assembly can potentially be useful as an agent to treat cancer.

Individual microtubules can be observed in the light microscope, and their lengths can be plotted as a function of time. It is known that microtubules switch randomly between growing and shrinking in a process known as dynamic instability. Both assembly and disassembly proceed at uniform rates, but there is a large difference between the rate of assembly and that of disassembly, as seen in the different slopes of the lines (Figure 1.3). During periods of growth, the microtubule elongates at a rate of 1 μm/min. Notice the abrupt transitions to the shrinkage stage (catastrophe) and to the elongation stage (rescue). The microtubule shortens much more rapidly (7 μm/min) than it

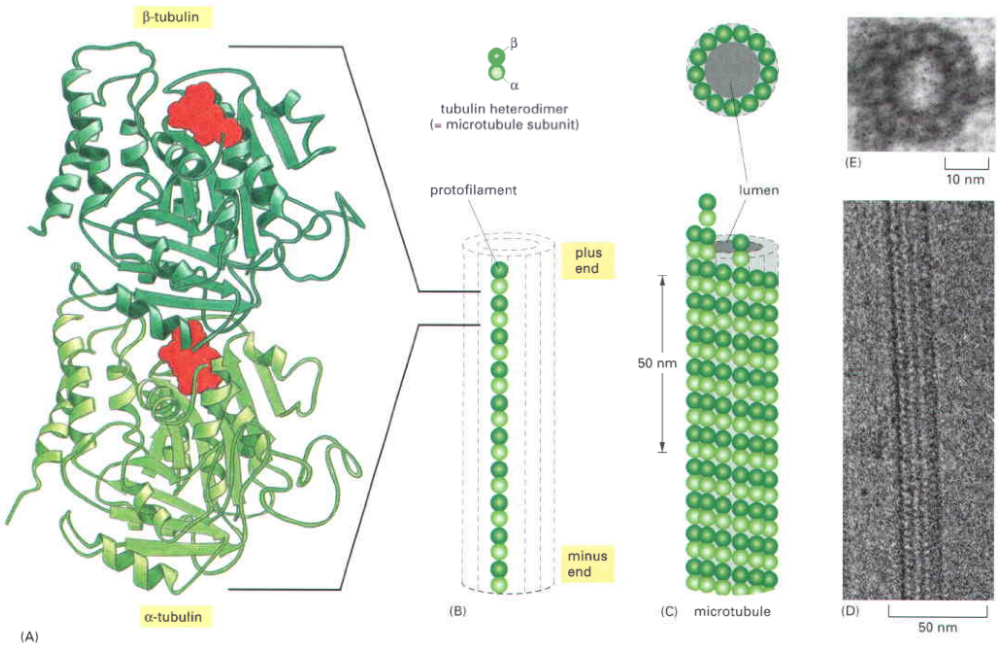

Figure 1.2 The structure of a microtubule and its subunit. (A) The subunit of each protofilament is a tubulin heterodimer, formed from a very tightly linked pair of α- and β-tubulin monomers. The GTP molecule in the α-tubulin monomer is so tightly bound that it can be considered an integral part of the protein. The GTP molecule in the β-tubulin monomer, however, is less tightly bound and has an important role in filament dynamics. Both nucleotides are shown in red. (B) One tubulin subunit (α-β heterodimer) and one protofilament are shown schematically. Each protofilament consists of many adjacent subunits with same orientation. (C) The microtubule is a stiff hollow tube formed from 13 protofilaments aligned in parallel. (D) A short segment of a microtubule viewed in an electron microscope. (E) Electron micrograph of a cross section of a microtubule showing a ring of 13 distinct protofilaments. (A, B, and C courtesy of Bruce Alberts et al. [7]; D, courtesy of Richard Wade; E, courtesy of Richard Link.)

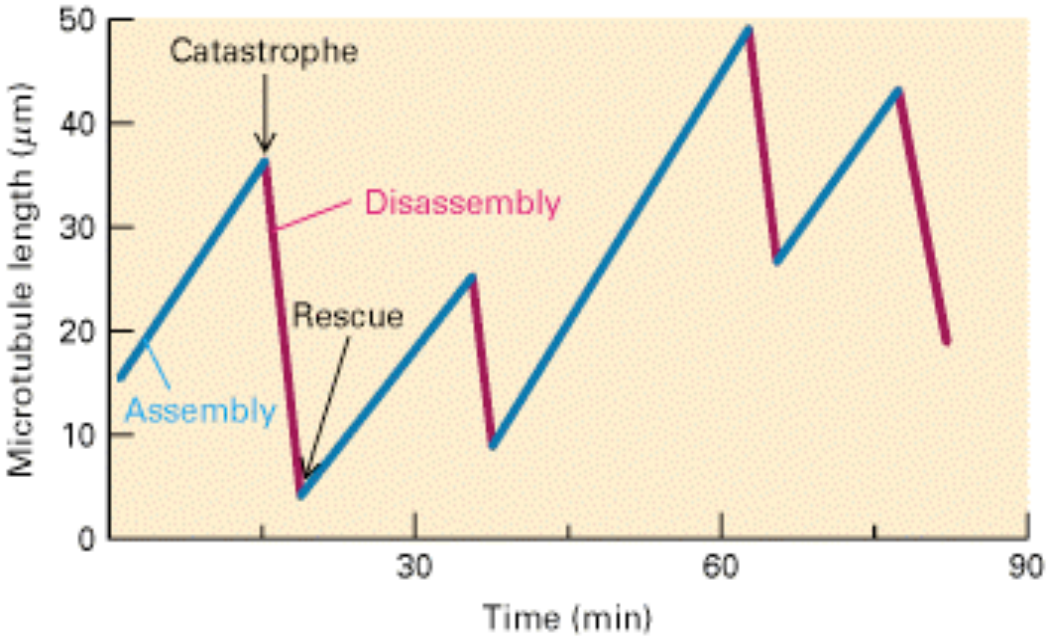

Figure 1.3 Dynamic instability of microtubules in vitro. Courtesy of P. M. Bayley, K. K. Sharma, and S. R. Martin, 1994, in Microtubules, Wiley-Liss, p. 119.

elongates.

Since the various filaments of the cytoskeleton exhibit mechanical properties of semi-flexible rods, they may also be subjected to mechanical oscillations which we briefly discuss next.

1.2 Oscillations

1.2.1 Damped Oscilations

In this section we consider the motion of a single particle under the influence

of a restoring force proportional to the distance of the particle from the origin and resistive force proportional to the velocity of the particle. Proportionality coefficients are considered as k and b, respectively. The differential equation of motion for such a particle is

$$m\ddot{x} = -kx - b\dot{x}. \tag{1.1}$$

Solution of the above equation depends on the relative values of k/m and $b/2m$ which for simplicity are called ω_0 and β, respectively.

If $\omega_0 > \beta$, the motion is called underdamped. The solution for the underdamped motion is

$$x(t) = A\exp(-\beta t)\cos(\omega_1 t - \delta), \tag{1.2}$$

where

$$\omega_1 = (\omega_0^2 - \beta^2)^{1/2}. \tag{1.3}$$

A and δ can be found from the initial conditions for position and velocity of the particle.

If $\omega_0 = \beta$, we will have the critical damped motion. Solution for this motion is

$$x(t) = (A + Bt)\exp(-\beta t). \tag{1.4}$$

Again A and B are found from the initial conditions of the particle. For a given set of initial conditions (here initial position and initial velocity of the particle), a critically damped oscillator (particle) will approach equilibrium at a more rapid rate than that for either an underdamped or an overdamped oscillator (particle).

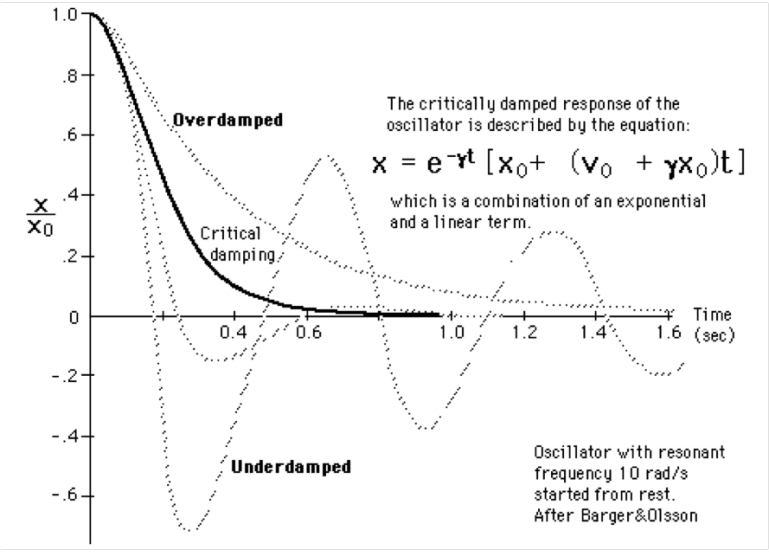

Figure 1.4 A graph for all three general cases for an oscillator: underdamped, overdamped, and critically damped motion.

When $\omega_0 < \beta$, the motion is called overdamped. The solution for the overdamped motion is

$$x(t) = \exp(-\beta t)[A\exp(\omega_2 t) + B\exp(\omega_2 t)], \tag{1.5}$$

where

$$\omega_2 = (\beta^2 - \omega_0^2)^{1/2}. \tag{1.6}$$

Figure 1.4 shows a graph of all three general cases.

1.2.2 Driven Oscillations: Sinusoidal Driving Forces

In Section 1.2.1 we obtained the solution for free oscillations of a particle

(or equivalently oscillation of charges in the RLC circuit). Generally, after a few oscillations, the particle asymptotically stops due to dissipation of the energy which comes from the resistive force.

In order to keep the oscillations alive, we need to pump the energy to the system which in this case will be called a driven oscillation. A fundamental case for the driven oscillation is when the driving force is a sinusoidal force. The reason is that we can expand any driving force in terms of a superposition of sinusoidal forces with different frequencies. Note that there is no need that the force be periodic.

The differential equation of motion for a particle which is driven by a sinusoidal force of $F_0 \cos \omega t$ in addition to the restoring force and resistive force is

$$m\ddot{x} = -kx - b\dot{x} + F_0 \cos \omega t, \tag{1.7}$$

which for simplicity can be written as

$$\ddot{x} + 2\beta\dot{x} + \omega_0 x = A \cos \omega t, \tag{1.8}$$

where $A = F_0/m$.

Solution of Eq. (1.8) consists of two parts. The first part is a complementary function which is basically the free oscillation solution which has been written in the previous section. The second part is the particular solution. For the particular solution we try the following function:

$$x_p(t) = D \cos(\omega t - \delta). \tag{1.9}$$

For finding A and δ we put the above function in Eq. (1.8). Using the fact

that $\sin\omega t$ and $\cos\omega t$ are linearly independent, with some simple algebra we have [8]

$$x_p(t) = \frac{A}{[(\omega_0^2 - \omega^2)^2 + 4\omega^2\beta^2]^{1/2}} \cos(\omega t - \delta), \tag{1.10}$$

with

$$\delta = \tan^{-1}(\frac{2\omega\beta}{\omega_0^2 - \beta^2}). \tag{1.11}$$

For large t, compared with the period of free oscillations, the particular (or steady state) solution will be the only important term.

A very important quantity in a driven oscillation is the resonance frequency. Resonance frequency, ω_R, is the frequency which maximizes the amplitude of the oscillator, D, with a constant amplitude for the driving force, A.

Differentiating the amplitude in Eq. (1.10) with respect to ω and setting the result to zero gives the resonance frequency,

$$\omega_R = (\omega_0^2 - 2\beta^2)^{1/2}. \tag{1.12}$$

The quantity which describes the degree of damping (or sharpness of resonance) in an oscillating system is called the quality factor (Q factor) of the system. Q factor for the system can be found with the following quantity:

$$Q = \frac{\omega_R}{2\beta}. \tag{1.13}$$

Figure 1.5 shows the resonance curves for several different values of the Q factor.

In order to expand the theory of oscillation from a single particle, which we discussed in this section, to continuous systems such as rods (or beams), we briefly review the beam theory in the next section.

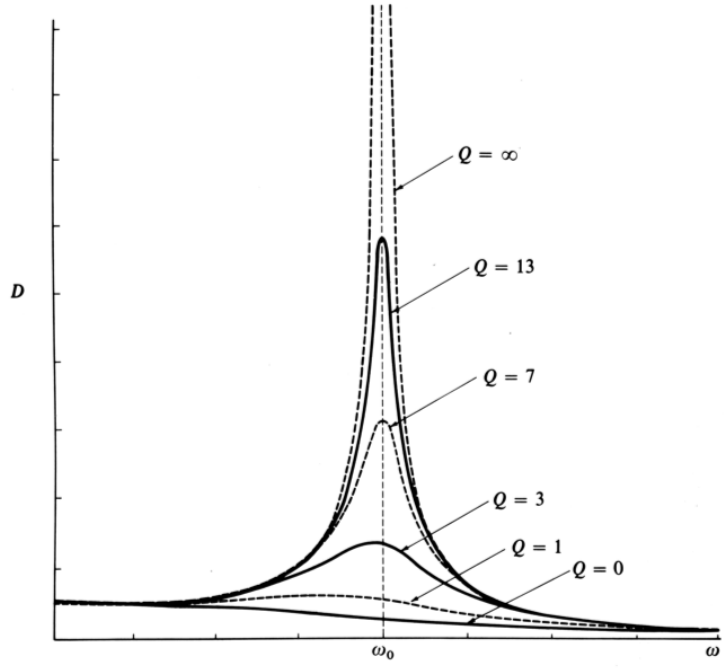

Figure 1.5 Resonance curves for several different values of Q factor. Courtesy of Jerry B. Marion [8].

1.3 Beam theory

"Beam theory began with Galileo Galilei (1564-1642), who investigated the behavior of various types of beam. His work on mechanics of materials is described in his famous book "Two New Sciences", first published in 1638 [9]. Although Galileo made many important discoveries regarding beams, he did not correctly obtain the distribution of stresses in a beam. Further progress was made by Mariotte, Jacob Bernoulli, Euler, Parent, Saint-Venant, and others"[1] [11, 12].

1.3.1 Beam Equation

The relation between torque or bending moment, M, exerted on a rod and the curvature, k (which is the inverse of the radius of curvature ρ), of the bend is

$$M = \kappa k. \tag{1.14}$$

The above equation is called the beam equation and it is analogous to Hooke's law for a spring. Note that this equation is written locally, which means it relates the bending moment at the cross-section of a beam with the curvature of the beam at the same location in the beam. Figure 1.6 shows a schematic diagram of an element of the beam which is under the torque exerted on its cross-section . For simplicity, just a couple of forces in each cross-section have been shown instead of the distribution of the forces. The proportionality constant, κ, is called flexural rigidity. It can be proved that this constant

[1] This paragraph is taken from a book by J. M. Gere and S. P. Timoshenko [10].

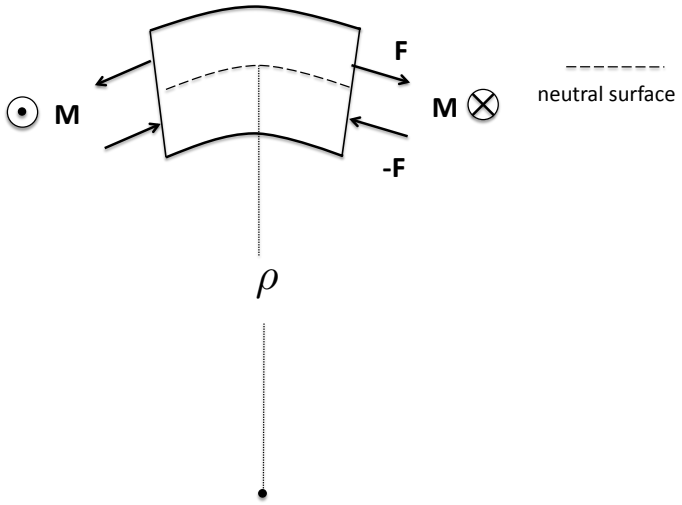

Figure 1.6 A schematic diagram of an element of a beam which is bent under the torque exerted on its cross section.

is actually a product of the second moment of the area (or more precisely the second moment of inertia of the area) of the beam's cross section, I, and the Young modulus of the filamentous material, E, thus, it is very common (especially in engineering literature) to write it as EI. An equation defining the second moment of area can be written as

$$I = \int y^2 da, \tag{1.15}$$

where y is the distance of the element with respect to neutral surface of the beam.

1.3.2 Curvature and Linear Beam Equation

In order to be able to solve the beam equation for the shape of the beam with a given bending moment we should use a coordinate system. There are several coordinate systems available which can be used to solve the beam equation but, we just use the Cartesian coordinate system in this thesis.

As is generally known the curvature of a flat curve, $y(x)$, at any point, x, in Cartesian coordinates can be written as [13]

$$k = \frac{d^2y/dx^2}{[1 + (dy/dx)^2]^{3/2}}, \tag{1.16}$$

and substituting the above equation into Eq. (1.14) gives

$$\frac{d^2y/dx^2}{[1 + (dy/dx)^2]^{3/2}} = \frac{M(x)}{EI}. \tag{1.17}$$

Unfortunately due to the non-linearity of Eq. (1.17), in most cases we are not able to solve it completely analytically. However, in most cases we are interested to solve it when the curvature of the beam is small. In this case, which is called the small angle approximation, we can neglect dy/dx in the denominator of Eq. (1.17) with respect to 1. In that case the beam equation will be reduced to

$$\frac{d^2y}{dx^2} = \frac{M(x)}{EI}. \tag{1.18}$$

1.3.3 Some Examples

For clarification of this equation we discuss a few examples at this stage. Figure 1.7 shows a schematic of a slender rod with length L which is fixed at its left end while a perpendicular force is exerted on its other end. The bending moment exerted on the rod at any point simply can be written as

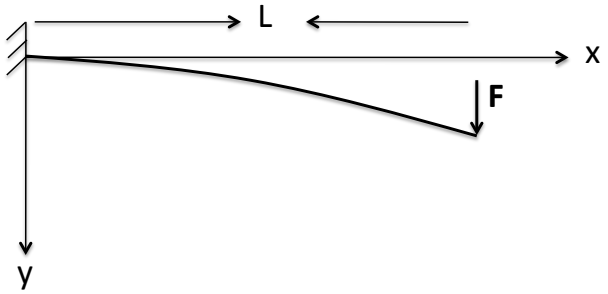

Figure 1.7 A schematic of a slender rod which is fixed at its left end while a perpendicular force is exerted on its other end.

$M(x) = F(L - x)$. Substituting this bending moment into Eq. (1.18) and integrating it twice gives

$$y(x) = \frac{F}{EI}(-\frac{x^3}{6} + \frac{Lx^2}{2}) + Ax + B, \tag{1.19}$$

for the equation of this beam. Using the boundary conditions for the fixed point for the function ($y(0) = 0$) and its derivative ($dy/dx|_0 = 0$) we can find the exact equation for the bent rod as

$$y(x) = \frac{Fx^2}{EI}(3L - x). \tag{1.20}$$

For the second example, we consider the slender rod in Figure 1.7 but this time force F has been uniformly distributed over the length of the rod. Again, we should calculate the bending moment exerted on each point of the rod first. The bending moment in this case is found from the following equation:

$$M(x) = \int_x^L (x' - x)\frac{F}{L}dx' = \frac{F}{2L}(x^2 + -2xL + L^2). \tag{1.21}$$

Substituting the above equation in the beam equation and integrating twice we find the equation for the bent rod [2],

$$y(x) = \frac{Fx^2}{24EIL}(6L^2 - 4xL + x^2). \tag{1.22}$$

In some cases the exerted force is not a point force, like in example one, but instead we have a distribution of forces on the filament, like in example two. Unlike in the latter example, however, the distribution is not uniform but it is a function of the position of each point in the rod (Figure 1.8). In those cases, the force density (force per unit of length of the beam) is given (or at least it is known in nature) as $f(x)$. With integrating the normal component of this force over the length of filament and putting the result in Eq. (1.18) we will find the following beam equation:

$$\frac{d^2y}{dx^2} = \frac{1}{EI}\int_x^L (x' - x) f_\perp(x') dx'. \tag{1.23}$$

With taking derivative of Eq. (1.23) with respect to x twice we obtain another form of the beam equation,

$$\frac{d^4y}{dx^4} = \frac{f_\perp(x)}{EI}. \tag{1.24}$$

As this differential equation is a fourth order differential equation, it is more difficult to deal with compared with the second order equation in Eq. (1.23), and it is not preferred to solve when the integration in Eq. (1.23) is possible to be performed. But in some cases, the force density is a function of the solution of the beam equation itself. In such cases Eq. (1.23) will be an

[2]For calculating the flexural rigidity of a MT with the method of hydrodynamic flow [14, 15], we need to know the deflection of the MT end from this equation.

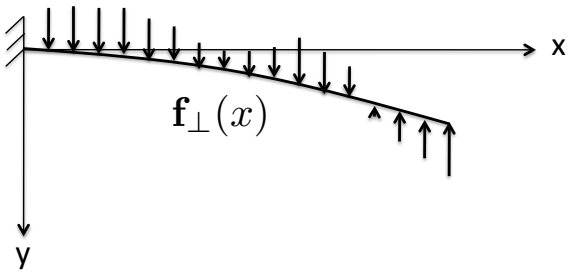

Figure 1.8 A schematic of a slender rod which is fixed at its left end while a continuous normal force density is exerted on it.

integral equation of the second kind, thus, in order to solve the beam equation we have to use Eq. (1.24)[3].

1.4 Thesis outline

In this thesis some theoretical properties of the bio- and nano-filaments are studied. In the first part of the thesis, by introducing a new experimental method and solving the problem completely analytically, we try to find a compact formula for the rigidity of these filaments by modeling the filaments as rigid rods. In the second part of this thesis, we try to solve the beam equation for the vibration of a microtubule with an ultrasound plane wave analytically.

[3]For calculating the flexural rigidity of a MT with relaxation method [16] we need to solve this equation with $f(x,t) = -c_\perp \partial y(x,t)/\partial t$.

-**Chapter 2** introduces a new method for measurement of flexural rigidity and cantilever stiffness of semiflexible bio-filaments and also nano-filaments. The method has several advantages over the other related methods and is easy to apply. The beauty of the method is the compact final formula which lets us evaluate the flexural rigidity with the measurement of only a few physical parameters of the filament.

-**Chapter 3** expands the theoretical formula for the flexural rigidity presented in the previous chapter taking into account the diameter of the filaments (which was neglected in chapter 2) by introducing a new parameter.

-**Chapter 4** investigates the interaction of the ultrasound plane waves with a simply attached microtubule at its two ends inside a viscous solution. Resonance conditions for the vibration of the microtubule is discussed in this chapter analytically.

-**Chapter 5** summarizes and concludes the work described in the thesis.

We have also included five appendices presenting mathematical details for some calculations.

Bibliography

[1] P. B. Moore and H. E. Huxley, and D. J. DeRosier, J. Mol. Biol. 50, 279-295 (1970).

[2] J. Squire, The Structural Basis of Muscular Contraction, Plenum Press, New York (1981).

[3] J. Howard, Mechanics of Motor Proteins and the Cytoskeleton, Sinauer Associates Inc., Sunderland, Massachusetts (2001).

[4] M. A. Geeves and K. C. Holmes, Annu. Rev. Biochem. 68, 687-728 (1999).

[5] D. Chretien, and R. H. Wade, Biol. Cell 71, 161-174 (1991).

[6] L. G. Tilney, J. Bryan, D. J. Bush, K. Fujiwara, M. S. Mooseker, D. B. Murphy, and D. H. Snyder, J. Cell Biol. 59, 267-275, (1973).

[7] B. Alberts, A. Johnson, J. Lewis, M. Raff, K. Roberts, P. Walter, Molecular Biology of the Cell, 5th ed., Taylor and Francis Group, New York (2008).

[8] J. B. Marion, Classical Dynamics of Particles and Systems, 2nd ed., Academic Press Inc., New York, New York (1970).

[9] G. Galilei, Dialogues Concerning Two New Sciences, translated from the Italian and Latin into English by Henry Crew and Alfonso De Salvio, The Macmillan Company, New York, (1933).

[10] J. M. Gere and S. P. Timoshenko, Mechanics of Materials, 3rd SI ed., Chapman and Hall, London (1991).

[11] S. P. Tomoshenko, History of Strength of Materials, Dover Publication Inc., New York (1983).

[12] I. Todhunter and K. Pearson, A History of the Theory of Elasticity and of the Strength of Materials, Dover Publications Inc., New York (1960).

[13] L. A. Segel, Mathematics Applied to Continuum Mechanics, Dover Publications Inc., New York (1987).

[14] P. Venier, A. C. Maggs, M.-F. Carlier, and D. Pantaloni, J. Biol. Chem. 269, 13353-13360 (1994).

[15] J. C. Kurz, and R. C. Williams, Jr., Biochemistry 34, 13374-13380 (1995).

[16] H. Felgner, R. Frank, and M. Schliwa, J. Cell Sci. 109, 509-516 (1996).

Chapter 2

A "Shooting-bead" Method for Finding the Flexural Rigidity of Semiflexible Rodlike Biological Filaments*

2.1 Introduction

When viewing the individual living cell as a nanomechanical and nanoelectronic device, we need to know what the physical properties of its internal hardware are. Interiors of living cells are structurally organized by the cytoskeleton networks of filamentous protein polymers: microtubules (MTs),

*A version of this chapter has been published. A. Samarbaksh and J. A. Tuszynski, Journal of Computational and Theoretical Nanosciences, Vol. 5, No. 10, p 2041-2044 (2008).

actin (microfilaments-MFs) and intermediate filaments (IFs) with motor proteins providing force and directionality needed for transport processes. F-actin can support large stresses [1] without a great deal of deformation and it ruptures at approximately 3.5 N/m^2. IFs have a rope-like structure composed of fibrous proteins consisting of two coiled coils and are mainly involved in the maintenance of cell shape and integrity. Ma et al [2] showed that IFs resist high applied pressures by increasing their stiffness. They can withstand higher stresses than the other two components without sustaining mechanical damage [1].

The cytoskeletal network of filaments has the responsibility of defining the cell shape, protecting the cell from changes in osmotic pressure, organizing its contents, providing cellular motility and finally is responsible for separating chromosomes during mitosis. The cytoskeleton is unique to eukaryotic cells and it acts as both muscle and skeleton, for movement and stability of the cell. With the exception of the cellulose fibers of the plant cell wall which are polysaccharides, the filaments of importance to the cell are all made up of protein polymers. Some cells, such as the auditory outer hair cells, contain strings of the protein spectrin. The extracellular matrix of connective tissue is traversed by fibers of collagen; a family of proteins exhibiting a variety of forms. Cells acquire their shape based on tensegrity principles due not only to the cytoskeleton's filaments but also from the extracellular matrix-the anchoring scaffolding to which cells are naturally secured in the body. Throughout the cell a network of contractile micro-filaments exerts tension and pulls the cell's membrane and all its internal constituents toward the nucleus at the core. Opposing this inward pull are two main types of compressive elements, one of which is outside the cell and the other inside. The component outside the cell

is called the extracellular matrix while the compressive "girders" inside the cell can be either MTs or large bundles of cross-linked micro-filaments within the cytoskeleton. The third component of the cytoskeleton, the IFs interconnect MTs and contractile microfilaments as well as linking to the surface membrane and the cell's nucleus. Contractile actin bundles act as molecular cables which exert a tensile force on the cell membrane and the internal constituents of the cell, pulling them all towards the nucleus. Simply put, MTs act as struts that resist the compressive force of the cables.

MTs are long hollow filaments made of $\alpha\beta$-tubulin dimers. These filaments have outer diameters measuring 25 nm and inner diameters of 15 nm. During cell division, tubulin can account for as much as 10% of the cell's protein. MTs form through the polymerization of $\alpha\beta$-tubulin heterodimers longitudinally arranged in a GTP-dependent process called dynamic instability. MTs are long hollow cylindrical objects made up of 12 to 17 protofilaments under *in vitro* conditions, and typically of 13 protofilaments *in vivo*. Each protofilament is shifted lengthwise with respect to its neighbour describing left-handed helical pathways around the MT. By biological standards, MTs are rigid polymers with a large persistence length [3] of 6 mm. From Janmey's experiments [1], MTs suffer a larger strain for a small stress compared to either MFs or IFs. The rupture stress for MTs [1] is very small and typically is only about 0.4-0.5 N/m^2. The lateral contacts between tubulin dimers in neighbouring protofilaments play a decisive role in MT stability, rigidity and architecture [4]. Tubulin dimers are relatively strongly bound in the longitudinal direction (along protofilaments), while the lateral interaction between protofilaments is much weaker [5]. There have been a number of theoretical [6,7] and experimental [8] studies in recent years dealing with the various aspects of the elasticity of MTs.

In this paper we propose a simple method of determining the stiffness of semi-flexible polymers such as MTs or F-actin or indeed bundles of such filaments [9] and provide a theoretical framework for interpreting the experimental results.

2.2 Theory and Calculation

In Figure 2.1 we show a schematic of a typical semiflexible rodlike biological filament, such as an actin filament or a microtubule, that at one end is clamped to a pivot point and the other free end has been pushed down by a bead inside an optical trap. Typical bead diameters are approximately 1 μm while the rod diameters range between 4 nm (actin) to 25 nm (MT's) or even 100 nm for MT bundles. In all these cases, however, the bead diameter is much larger than the diameter of the biopolymer. The cantilever stiffness of a rod with length of L is k and the radius of the bead is R.

Assuming that we can keep the rod in its bent conformation over a period of time, we can now imagine that if we suddenly turn the optical trap (laser tweezer) off, the force holding the rod down is abruptly removed. Hence, the bead that was pushing down on the free end of the rod while in the trap will now experience a reaction force from the tip of the rod leading to its displacement from its previous position. The amount of displacement a when moving the bead downward in the initial phase of the experiment will determine the initial position of the bead at the time of releasing it from the tip of the rod. Following the release of the bead from the laser trap, the bead will jump up. The motion of the bead can be analyzed in terms of two contributions that are described below.

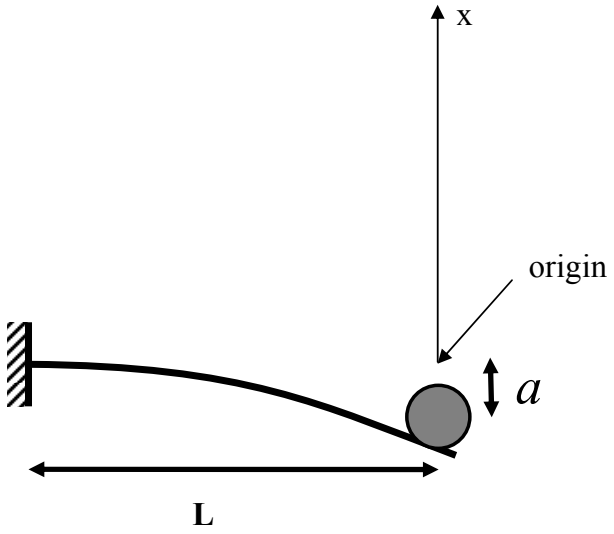

Figure 2.1 Schematic illustration of the rodlike biological filament pushed by a bead inside an optical trap.

2.2.1 Damped Harmonic Motion ($x \leq 0$)

The bead experiences two forces, an upward force (which is typically in the range of several pN) due to the cantilever stiffness of the rod and a downward viscous drag force. As mentioned above, we can assume the radius of the bead to be much greater than the radius of the rod and for simplicity we can ignore the viscous force exerted on the rod. Another reason that the viscous force exerted on rod is small compared with the viscous drag force exerted on the bead is that the velocity of all parts of the rod except the end is less than the velocity of the bead. Moreover, due to the forces experienced by the bead from the trap and then from the rod, we can ignore the effect of thermal fluctuations as negligible provided the energy stored in the deformed rod exceeds kT (the energy produced by several pN of force multiplied by

several nm of displacement will be sufficiently large). The equation of motion for the bead and its initial conditions are given below as

$$m\ddot{x} = -kx - 6\pi\eta R\dot{x}, \tag{2.1}$$

$$x(0) = -a, \quad \dot{x}(0) = 0. \tag{2.2}$$

Note that m and η represent the mass of the bead and viscosity of the solution, respectively. It has been assumed that the density of the bead is equal or close to the density of the solution (in most cases this will be composed mainly of water) which means that the buoyant force and the weight of the bead cancel each other out. Therefore, we need not make a correction for the apparent weight of the bead.

The solution of Equation (2.1) with initial condition (2.2) that corresponds to underdamped motion is well known [10] and we state it below as

$$x(t) = -a \exp\left(-\frac{3\pi\eta R}{m}t\right) \cos\left(\sqrt{\frac{k}{m} - \left(\frac{3\pi\eta R}{m}\right)^2}\, t\right). \tag{2.3}$$

The motion will be underdamped if the bead passes through the origin and this condition applies to a rigid rod and/or a light bead.

2.2.2 Damped Motion ($x \geq 0$)

The bead experiences just a downward viscous drag force. This motion starts from the moment when the bead passes through the origin at a time instant equal to $\pi/2\sqrt{\frac{k}{m} - \left(\frac{3\pi\eta R}{m}\right)^2}$ in part 2.2.1. The equation of motion of the bead and the initial conditions are

$$m\ddot{x} = -6\pi\eta R\dot{x}, \tag{2.4}$$

$$x(0) = 0, \quad \dot{x}(0) = a\sqrt{\frac{k}{m} - \left(\frac{3\pi\eta R}{m}\right)^2} \times \exp\left(-\frac{3\pi^2\eta R}{2m\sqrt{\frac{k}{m} - \left(\frac{3\pi\eta R}{m}\right)^2}}\right). \tag{2.5}$$

where for simplicity and without loss of generality we have assumed that the start time for the process is when the bead passes through the origin with velocity $\dot{x}(0)$ in Equation (2.5). The solution of Equation (2.4) with initial condition (2.5) is

$$x(t) = \frac{m\dot{x}(0)}{6\pi\eta R}(1 - \exp(-\frac{6\pi\eta R}{m}t)). \tag{2.6}$$

Asymptotically in time, the bead stops at distance d with respect to the origin (see Figure 2.2). How fast the bead approaches its final position depends on the value of $t_A = m/6\pi\eta R$ which will be referred to as the *asymptotic approach time constant*.

From Equation (2.5) and (2.6) with some simple algebra we readily find that

$$s\exp(s) = \frac{\pi a}{4d}. \tag{2.7}$$

Note that s is a dimensionless variable $3\pi^2\eta R/2m\sqrt{\frac{k}{m} - \left(\frac{3\pi\eta R}{m}\right)^2}$. Assuming the measurement of a and d is experimentally feasible, we can solve Equation (2.7) for s, then, using the definition of s and solving for k, the cantilever stiffness of the rod will be found as

$$k = \frac{9\pi^2\eta^2R^2}{m}\left(\frac{\pi^2}{4s^2} + 1\right). \tag{2.8}$$

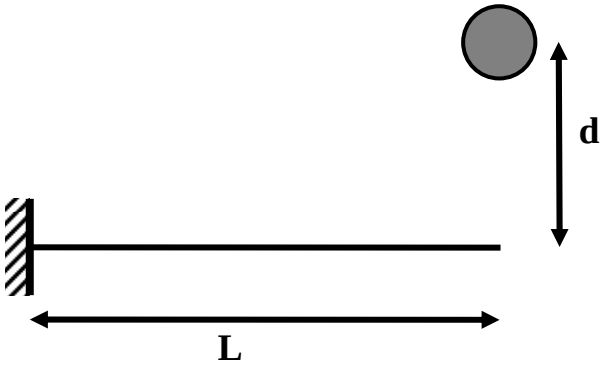

Figure 2.2 The final distance of the bead when it asymptotically comes to rest with respect to the origin.

To find the cantilever stiffness directly in terms of a/d we need to invert Equation (2.6) and substitute it into Equation (2.8),

$$k = \frac{9\pi^2\eta^2R^2}{m}\left(\frac{\pi^2}{4W^2\left(\frac{\pi a}{4d}\right)}+1\right). \tag{2.9}$$

Note that W is the *Lambert W* function [11].

For small deflections with respect to the length of the filament, using the Euler-Bernoulli bending formula [12] for homogeneous filaments we can relate the cantilever stiffness of the filament to its flexural rigidity [8] EI as

$$EI = \frac{1}{3}kL^3 = \frac{3\pi^2\eta^2R^2L^3}{m}\left(\frac{\pi^2}{4W^2\left(\frac{\pi a}{4d}\right)}+1\right). \tag{2.10}$$

Figure 2.3 shows the dependence of the *dimensionless flexural rigidity* as a function of a/d. $(EI)_0$ is a constant equal to $3\pi^2\eta^2R^2L^3/m$ that depends on the viscosity of the solution, the radius of the bead and the length of the filament.

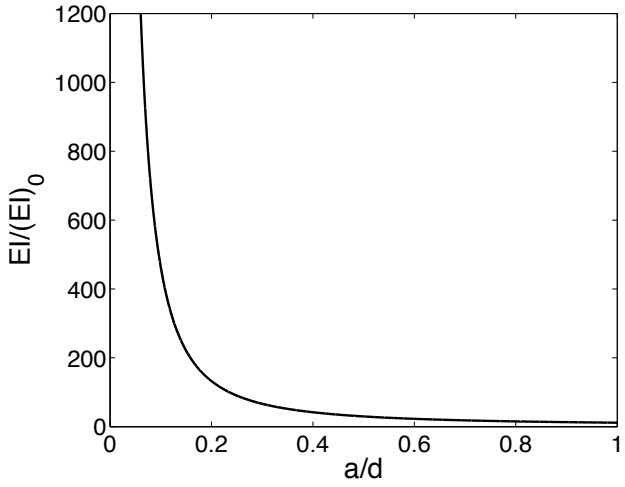

Figure 2.3 Dimensionless flexural rigidity $EI/(EI)_0$ as a function of a/d.

2.2.3 Stiff Filament Approximation

For stiff filaments we have $a/d \ll 1$ and we can keep just the first term of the expansion of se^s in Equation (2.7). In that case, the rod's flexural rigidity can be found from the following formula as

$$EI = \frac{3\pi^2\eta^2 R^2 L^3}{m}\left(\frac{4d^2}{a^2}+1\right). \tag{2.11}$$

Figure 2.4 shows the *dimensionless flexural rigidity* as a function of the ratio of a/d for the exact solution (dotted line) and in the stiff filament approximation (solid line).

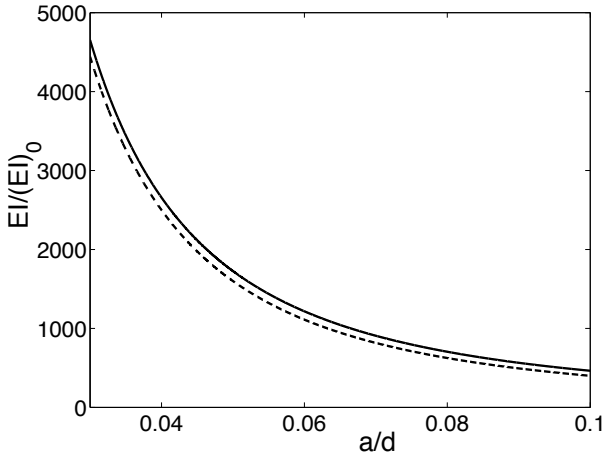

Figure 2.4 A plot of the dimensionless flexural rigidity $EI/(EI)_0$ as a function of a/d. The dotted line is the exact solution and the solid line represents the stiff filament approximation solution.

2.3 Conclusions

In conclusion, we note that this method offers numerous advantages over the other methods currently in use (e.g. the buckling force method [13,14], the hydrodynamic flow method [15,16], the wiggle and relaxation methods [17,18], or the thermal fluctuation technique [19]). We list the following reasons for advocating the use of the new method:

(a) For this experiment, the bead need not be attached to the filament as the attachment of the bead poses numerous technical problems. Hence the beads need not be coated as most of the time the beads do not attach to the filament. Actually, this was one of the reasons that guided us to the introduction of the proposed method.

(b) We need to use a microscope with only a single trap (for buckling force measurements one needs double traps).

(c) There is no need to find the force exerted on the bead by the trap (since only the measurement of the distance between the centre of the beam and the centre of the bead is required).

(d) There is no need to know the exact shape of the filament (which is required for the buckling force and the thermodynamic fluctuation methods).

(e) There is no need to oscillate the trap (like in the wiggle method).

(f) There is no need to measure the time (as in the relaxation method).

(g) There is no need to measure the velocity of the bead or the rod (as in the hydrodynamic flow method).

(h) The only measurement that we need to perform is the measurement of the length for a and d. It can be easily appreciated that the measurement of length is more straightforward and accurate than the measurement of time or velocity, especially at the nanoscale.

(i) Finally, because the ratio of a/d is important not a and d individually, there is no need to calibrate the monitor of the microscope.

In the next chapter we will modify the shooting bead formula to take into account the effects of the viscous drag force exerted on the filament by defining a key variable, called the filament energy-loss factor (or filament drag factor), that accounts for all the energy-loss effects.

Bibliography

[1] P. A. Janmey, U. Euteneuer, P. Traub, and M. Schliwa, J. Cell Biol. 113, 155 (1991).

[2] L. Ma, J. Xu, P.A. Coulombe and D. Wirtz, J. Biol. Chem. 274, 19145 (1999).

[3] D. Boal, Mechanics of the Cell, Cambridge University Press, Cambridge, (2002).

[4] P. Meurer-Grob, J. Kasparian and R. H. Wade, Biochemistry 40, 8000 (2001).

[5] A. Kis, S. Kasas, B. Babic, A. J. Kilik, W. Benoit, G. A. D. Briggs and C. Schonenberger, S. Catsicas, and L. Forr, Phys. Rev. Lett. 89, 248101 (2002).

[6] J. A. Tuszynski, T. Luchko, S. Portet, and J. M. Dixon, Eur. Phys. J. E 17, 29-35 (2005).

[7] S. Portet, J. A. Tuszynski, C. M. Hogue, and J. M. Dixon, Eur. Biophys. J., 34, Number 7, 912-920 (2005).

[8] J. Howard, Mechanics of Motor Proteins and the Cytoskeleton, Sinauer Associates Inc., Sunderland, Massachusetts (2001).

[9] O. Lieleg, M. M. A. E. Claessens, C. Heussinger, E. Frey, and A. R. Bausch, Phys. Rev. Lett. 99, 088102 (2007).

[10] J. B. Marion, Classical Dynamics of Particles and Systems, 2nd ed., Academic Press Inc., New York, New York (1970).

[11] Mathematical Review, American Mathematical Society (1940).

[12] L. A. Segel, Mathematics Applied to Continuum Mechanics, Dover Publications Inc, New York (1987).

[13] M. Kikumoto, M. Kurachi, V. Tosa, and H. Tashiro, Biophysical Journal, 90, 1687-1696 (2006).

[14] M. Kurachi, M. Hoshi, and H. Tashiro, Cell Motil. Cytoskeleton, 30, 221-228 (1995).

[15] P. Venier, A. C. Maggs, M.-F. Carlier, and D. Pantaloni, J. Biol. Chem. 269, 13353-13360 (1994).

[16] J. C. Kurz, and R. C. Williams, Jr., Biochemistry. 34, 13374-13380 (1995).

[17] H. Felgner, R. Frank, and M. Schliwa, J. Cell Sci. 109, 509-516 (1996).

[18] H. Felgner, R. Frank, J. Biernat, E.-M. Mandelkow, E. Mandelkow, B. Ludin, A. Matus, and M. Schliwa, J. Cell Biol. 138, 1067-1075 (1997).

[19] F. Gittes, B. Mickey, J. Nettleton, and J. Howard, J. Cell Biol. 120, 923-934 (1993).

Chapter 3

Viscous Drag Effect in the Flexural Rigidity and Cantilever Stiffness of Bio- and Nano-filaments Measured with the Shooting-bead Method*

3.1 Introduction

Interiors of living cells are structurally organized by the cytoskeleton networks of filamentous polymers whose bio-mechanical properties are of key in-

*A version of this chapter has been published. A. Samarbaksh and J. A. Tuszynski, Physical Review E, Vol 80, 011903 (2009) DOI: 10.1103/PhysRevE.80.011903. Also selected for the July 13, 2009 issue of Virtual Journal of Nanoscale Science and Technology.

terest to biophysicists. With few exceptions, the filaments of importance to the cell are all made up of protein polymers. Protein filaments of the cytoskeleton consist of: actin (microfilaments-MFs), intermediate filaments (IFs) and microtubules (MTs). Throughout the cell a network of contractile actin bundles exerts tension and pulls the cell's membrane toward the nucleus at the core. MTs resist the compressive force of the actin cables providing a balance. IFs provide additional structural stability.

Microfilaments are single-stranded filaments, with diameters of approximately 3-6 nm and variable lengths. Microfilaments are found linked together by actin-associated proteins and congregate into one of three major forms. There are over 100 different actin-binding proteins responsible for actin associating with the membrane, with membrane-bound receptors, and with ion channels, as well as for promoting assembly and causing the depolymerization of those filaments. Actin-binding proteins, such as ARP2/3 and profilin, regulate micro-filament assembly. Actin depolymerizing factor (ADF)/cofilin stimulates disassembly. Gelsolin caps fast-growing ends of filaments and may also be involved in filament disassembly.

Microtubules are long hollow filaments consisting of bound α-tubulin and β-tubulin monomers. MT polymerization can be controlled by temperature, pH, concentration of protein and ions to produce closely or widely spaced MTs, centers, sheets, rings and even the so-called macrotubes that have diameters in the range of 200-500 nm and are polymerized with the influence of an elevated zinc ion concentration [1]. Assembled microtubules have outer diameters of 25-26 nm and inner diameters of 15 nm and typically contain 13 protofilaments when assembled *in vivo*. MTs are made up of 12 to 17 protofilaments under *in vitro* conditions. Each protofilament is shifted lengthwise with respect to its

neighbor describing left-handed helical pathways around the MT. Like actin filaments, microtubules have plus- and minus-ends. Polymerization or elongation occurs preferentially at plus-ends and depolymerization or shortening occurs at minus-ends. Microtubule associated proteins (MAPs) are tissue- and cell type-specific and represent several classes with different functions. General classes are minus-end binding, plus-end binding (e.g., the kinetochore of mitotic chromosomes, polymer severing, polymer stabilizing) and cross-linking (i.e., MAP-2 and tau in neurons), and motor proteins. These microtubule binding proteins determine the architecture of microtubules and microtubule assemblies.

All of the above cellular protein filament structures have significant persistence lengths that increase with the molecular mass of the building block and a related mechanical stability and rigidity that is of growing interest to physicists. F-actin can support large stresses [2] without a great deal of deformation and it ruptures at approximately 3.5 N/m^2. Ma et al [3] showed that IFs resist high applied pressures by increasing their stiffness. They can withstand higher stresses than the other two components without sustaining mechanical damage [2]. By biological standards, MTs are rigid polymers with a large persistence length [4] of 6 mm. From Janmey's experiments [2], MTs exhibit a larger strain for a small stress compared [3] to either MFs or IFs. The rupture stress for MTs is very small and typically is only about 0.4-0.5 N/m^2. The lateral contacts between tubulin dimers in neighboring protofilaments play a decisive role in MT stability, rigidity and architecture [5]. Tubulin dimers are relatively strongly bound in the longitudinal direction (along protofilaments), while the lateral interaction between protofilaments is much weaker [6]. There have been a number of theoretical [7, 8] and experimental [9] studies in recent

years dealing with the various aspects of the elasticity of MTs.

In this thesis we propose a simple method of determining the stiffness of semi-flexible polymers such as MTs or indeed bundles of such filaments [10] and provide a theoretical framework for interpreting the experimental results. One of the main issues in this paper is not only the analysis of the shooting-bead method [11] as applied to the nano- and bio-filaments but, more specifically, how the drag forces exerted on the filament present in the viscous medium affect the energy loss and consequently the measurement's results. This method is especially suited for stiff filaments or their bundles (e.g. cilia, flagella, macrotubes or MAP-interconnected MT bundles in axons). Even for individual microtubules, where Taute et al [12] determined that filament drag is a major effect for the bending of MT's, the length of the filament makes a crucial difference to the cantilever stiffness such that short MT's become stiffer and the resultant motion of the bead is underdamped making the method applicable. Moreover, the method described below can be readily utilized for nanotechnologically produced filaments such as single-walled or multi-walled carbon nanotubes (CNTs) [13] which provide an excellent system for calibration and control.

3.2 Conceptual Basis

In Figure 3.1 we show a schematic of two states of a typical semi-flexible rod-like bio- or nano-filament, that is clamped at one end to a pivot point and whose other (free) end, first has been pushed down by a bead inside an optical trap [14, 15] and then has been released by turning the laser trap off. The

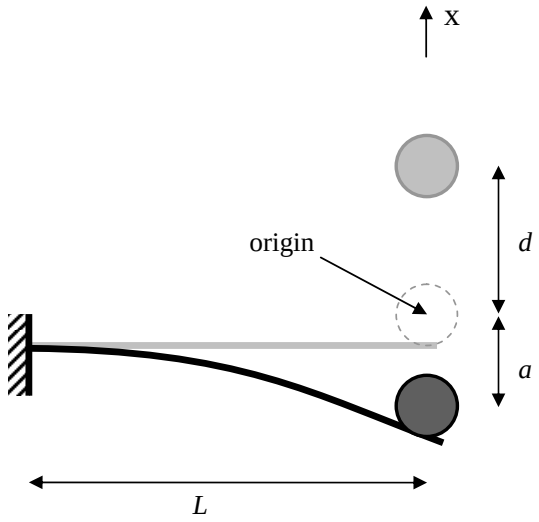

Figure 3.1 Schematic illustration of the two states of the rod-like biological filament and the bead. First, the filament has been pushed by a bead inside an optical trap and second, the filament has been released and the bead has come to rest asymptotically. (Figure not to scale, usually a, d, and R are much smaller than L).

cantilever stiffness of a rod with length L is k and the radius of the bead is denoted as R. Typical bead diameters are approximately 1-2 μm (with focused laser, it is possible to trap beads with a radius as low as 200 nm), while the rod diameters range between 100 nm for microtubule bundles, 200-500 nm for macrotubes and about 500 nm for cilia. Also nanotechnology methods allow to make filaments from different materials with controlled values of their radii. For example, it is now possible to make single-walled or multi-walled carbon nanotubes (CNTs) with different radii ranging from a few to 100 nm.

In this chapter, our primary aim is to expand the proposed method for measuring filament stiffness in order to include the effects of the energy loss due to the viscous drag force exerted on the filament itself and to make the final

shooting-bead formula as accurate as possible. While the commonly employed wormlike chain model has become standard in the description of semi-flexible and flexible polymers such as DNA, this is not a necessary level of approximation for stiffer filaments which have long persistence length such as MTs, cilia, flagella or CNTs where small deflection approximation can be warranted. For example, the mm-range persistence lengths and a high level of rigidity characteristic of MT 's translate into a picture where a significant thermal fluctuation in shape occurs over tens to hundreds of thousands of constituent dimers. In this chapter we also wish to provide a means of estimating experimental errors for the shooting-bead formula and assess under which instrumental resolution this method will be able to work. To make the paper self-contained and use the results of the intermediate steps yielding the first shooting-bead formula [11] (when the bead's diameter is much larger than that of the rod), in this section we briefly explain the concepts involved in the method.

Assuming that we can keep the rod in its bent conformation over a certain period of time, we can now imagine that if we suddenly turn the optical trap (laser tweezer) off, the force holding the rod down is abruptly removed. Hence, the bead that was pushing down on the free end of the rod while in the trap will now experience a reaction force from the tip of the rod leading to its displacement from its previous position. The amount of displacement a when moving the bead downward in the initial phase of the experiment will determine the initial position of the bead at the time of releasing it from the tip of the rod. Following the release of the bead from the laser trap, the bead will jump up. The motion of the bead can be analyzed in terms of two contributions. First, the bead experiences two forces, an upward force due to the cantilever stiffness of the rod and a downward viscous drag force (there

are two other forces; Appendix A provides an additional explanation of the effects created by these forces). The equation of motion for the bead together with the initial conditions is given below:

$$m\dot{x} = -kx - 6\pi\eta R\dot{x}, \quad x(0) = -a, \quad \dot{x}(0) = 0. \tag{3.1}$$

Note that m and η represent the mass of the bead and viscosity of the solution, respectively. The solution of Equation (3.1) with the initial conditions that corresponds to underdamped motion is [16]

$$x(t) = -aexp\left(-\frac{3\pi\eta R}{m}t\right)\cos\left(\sqrt{\frac{k}{m} - \left(\frac{3\pi\eta R}{m}\right)^2}\,t\right). \tag{3.2}$$

The motion will be underdamped if the bead passes through the origin and this condition applies to a rigid rod and/or low viscous solution[1]. In the second part of the motion ($x \geq 0$), the bead experiences just a downward viscous drag force. This motion starts from the moment when the bead passes through the origin at a time instant equal to $t_0 = \pi/2\sqrt{\frac{k}{m} - \left(\frac{3\pi\eta R}{m}\right)^2}$ in the first part of the motion. As a result, the equation for the bead's position as a function of time is [11]

[1]Theoretically it is always possible to have an underdamped motion for the bead by making the value of the quantity under the square root in Equation (3.2) positive. Even if we don't have an underdamped motion for the bead at the beginning, by cutting the filament to a shorter length we can make k large enough (as we know, k is inversely proportional to the third power of the length of the filament) to end up with a positive value for the quantity under the square root.

$$x(t) = \frac{ma}{6\pi\eta R}\sqrt{\frac{k}{m} - \left(\frac{3\pi\eta R}{m}\right)^2}\exp\left(-\frac{3\pi^2\eta R}{2m\sqrt{\frac{k}{m} - \left(\frac{3\pi\eta R}{m}\right)^2}}\right)\left(1 - \exp\left(-\frac{6\pi\eta R}{m}t\right)\right). \tag{3.3}$$

Note that in the above equation we have shifted our initial time from $t = t_0$ to $t = 0$. Since $x(t \to \infty) = d$ (due to the exponential dependence of $x(t)$ on t, just after passing a few intervals of $\tau = m/6\pi\eta R$, *asymptotic approach time constant*, we can consider the bead as being at rest) solving Equation (3.3) for k and using the Euler-Bernoulli bending formula [17] for small deflection, we can find the following formula (which will be referred to as the first shooting-bead formula) for flexural rigidity[2] of the filament:

$$\kappa = \frac{1}{3}kL^3 = \frac{9\pi\eta^2 L^3}{4\rho R}\left(\frac{\pi^2}{4[W\left(\frac{\pi a}{4d}\right)]^2} + 1\right). \tag{3.4}$$

Note that the symbol W in the above equation is called the *Lambert W* function[3] [18]. Since it is easier to determine the density of the bead, ρ, compared to its mass, we have changed our variable from mass of the bead to its density at this final point. This will also help in reducing the error when calculating the error propagation for our formula if the original information is based on the knowledge of the density and radius of the bead.

To simplify the notation, we define the following new variables for future calculations:

[2]As flexural rigidity (or bending stiffness) is the product of the Young modulus, E, of the filament material and the second moment of area, I, of the filament cross-section, it is very common to use EI instead of κ for flexural rigidity.

[3]It is also called the omega function or product logarithmic function.

$$\Lambda = \frac{3\pi\eta R}{m}, \qquad \Omega = \sqrt{\frac{k}{m} - \left(\frac{3\pi\eta R}{m}\right)^2}. \tag{3.5}$$

3.3 Energy Conservation and Filament Energy-Loss Consideration

In Section 3.2 the problem at hand has been solved analytically by including the net force exerted on the bead but ignoring the force exerted on the filament by the solution. It is a good idea to investigate our solution from the conservation of energy point of view at this stage. Since this part can be considered as a totally separate part and in order to maintain the main flow of the paper, this part has been moved to the appendix. The interested reader can see the proof in Appendix B.

Looking at the problem from the energy point of view will guide us to define a very important parameter that can help us to provide an estimate of the energy-loss due to the viscous force exerted on the filament based on the bead's energy-loss.

In this section we intend to estimate the energy-loss of the filament (Q_{1R}) and compare it with the energy-loss of the bead (Q_{1B}) and the total energy-loss (Q_{1T}) during the first part of the motion. To solve the problem analytically we approximate the motion of the bent filament as a rotating rod with the length of $L/2$ (see Figure 3.2). This is a good approximation because for a small deflection, the area swept by the rod compared to the area swept by the whole filament amounts to more than 2/3 (see Appendix C for a mathematical

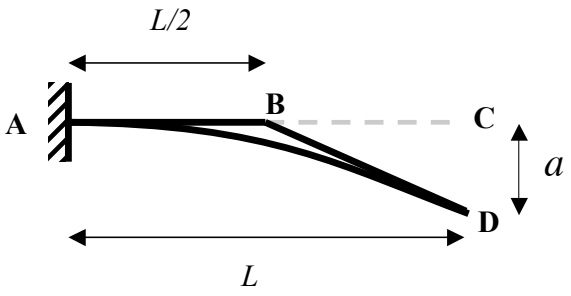

Figure 3.2 Representation of the filament as a rotating rigid rod with the length of $L/2$. (deflection angle CBD is exaggeratedly shown).

proof of this statement).

The viscous drag torque exerted on the rod (BD) with radius r that rotates with angular velocity ω inside a medium with viscosity η is equal to [9]

$$T = \frac{\frac{1}{6}\pi\eta L^3}{\ln(\frac{L}{2r}) - 0.66}\,\omega. \tag{3.6}$$

The infinitesimal energy-loss of the rod when it rotates by $d\theta$ is therefore

$$dQ_{1R} = \frac{\frac{1}{6}\pi\eta L^3}{\ln(\frac{L}{2r}) - 0.66}\,\omega d\theta = \frac{\frac{1}{6}\pi\eta L^3}{\ln(\frac{L}{2r}) - 0.66}\,\omega^2 dt. \tag{3.7}$$

Here dt denotes the elapsed time for such an infinitesimal rotation.

As we know, the tip of the filament pushes on the bead which means that the velocity of the tip is the same as the velocity of the bead at any time during the first part of the motion. Thus using $v = L\omega/2$ we find

$$dQ_{1R} = \frac{\frac{2}{3}\pi\eta L}{\ln(\frac{L}{2r}) - 0.66}\,v^2 dt. \tag{3.8}$$

To calculate the energy-loss of the rod we have to integrate an expression based on Equation (3.8) but at this stage we can not do this yet because the

equation of motion for the bead (the system composed of the bead and the filament) does not remain the same as before (when we ignored that filament energy-loss). For this reason we just find the ratio of the filament's energy-loss to the bead's energy-loss at the moment as this ratio plays an important role in our calculation. Namely,

$$\frac{Q_{1R}}{Q_{1B}} = \frac{\int dQ_{1R}}{\int dQ_{1B}} = \frac{1}{9\frac{R}{L}(\ln(\frac{L}{2r}) - 0.66)} = \alpha - 1. \tag{3.9}$$

Therefore, knowing the radius of the filament, the length of the filament and the radius of the bead α can be found. Note also that α is the ratio of the total energy-loss to the bead energy-loss which has a value greater than one and we refer to it as the *filament energy-loss factor* or *filament drag factor*.

Figure 3.3 shows the filament energy-loss factor as a function of the filament radius for a 10-μm-long filament and $1\mu m$ bead diameter. It should be stressed that although we have found the ratio of Q_{1R}/Q_{1B}, we are not able to calculate the filament energy-loss at this stage. The reason for this is that Q_{1B} does not remain the same as before in the case when filament energy-loss is ignored [see Equation (B.4) or Equation (B.7) in Appendix B]. This means that the following relation is not correct.

$$Q_{1R} = (\alpha - 1)Q_1 = \frac{1}{2}(\alpha - 1)ma^2\Lambda^2(\frac{\pi^2}{4[W(\frac{\pi a}{4d})]^2}(1 - \exp(-2W(\frac{\pi a}{4d}))) + 1). \tag{3.10}$$

To calculate the correct filament energy-loss we first need to evaluate the new equation of motion (that will be solved in the next section), then we need to follow all the steps that we took to reach Equation (B.4) or Equation (B.7) for finding a new solution.

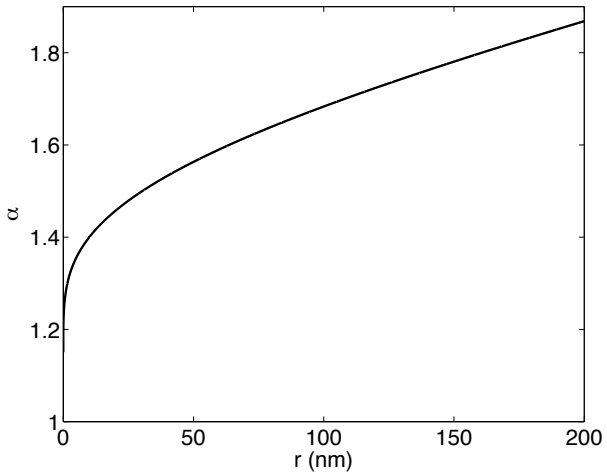

Figure 3.3 Filament energy-loss factor as a function of filament radius for a 10 μm filament and a 1 μm bead diameter.

3.4 Effects of Filament Energy-Loss on Dimensionless Flexural Rigidity Curve

In this section we derive two equations for calculating the cantilever stiffness and flexural rigidity with consideration of filament energy-loss. The equation of motion for the system (bead + filament) is

$$(I_B + I_R)\ddot{\theta} = -k(\frac{L}{2})^2\theta - \frac{\frac{1}{6}\pi\eta L^3}{\ln(\frac{L}{2r}) - 0.66}\dot{\theta} - 6\pi\eta(\frac{L}{2})^2\dot{\theta}. \tag{3.11}$$

Here, θ is the angle between the rod and the undeflected filament (the angle between BD and BC in Figure 3.2). Assuming that r, a and R are all much smaller than L and using the definition of the filament energy-loss factor, the

above equation becomes

$$\frac{I_B + I_R}{(\frac{L}{2})^2}\ddot{\theta} = -k\theta - 6\pi\eta\alpha R\dot{\theta}. \tag{3.12}$$

Using the moment of inertia for a single particle (keeping in mind that the radius of the bead is much smaller than the length of the filament) with mass m and moment of inertia for a rigid rod with length $L/2$ and mass m_R as well as the relation between x and θ ($x = L\theta/2$) we obtain

$$(m + \frac{1}{3}m_R)\ddot{x} = -kx - 6\pi\eta\alpha R\dot{x}. \tag{3.13}$$

Generally 1/6 of the mass of the filament is much smaller than the mass of the bead. For example, even for a solid filament (many bio-filaments or bundles of them can be considered to have hollow interiors such as microtubules or macrotubes) with a radius of 100 nm (that would be a very thick filament) and with a 10 μm length and the density of water, the effect of ignoring the mass of the filament with respect to the mass of the bead with a radius of 1 μm and the same density is just 3.75%. Now, comparing the above equation with Equation (3.1) and eliminating m_R, we notice that the only difference between these equations amounts to the replacement of η with $\alpha\eta$. It means that we can use the solution of that equation (with the same initial conditions) as a solution of Equation (3.13) where η is rescaled to become $\alpha\eta$.

Defining the following new variables,

$$\Lambda' = \frac{3\pi\alpha\eta R}{m}, \qquad \Omega' = \sqrt{\frac{k}{m} - \Big(\frac{3\pi\alpha\eta R}{m}\Big)^2}, \tag{3.14}$$

we find

$$x(t) = -a\exp(\Lambda' t)\cos(\Omega' t). \tag{3.15}$$

It is clear that the second part of the motion of the bead when it passes through the origin will satisfy the same differential equation of motion but this

time the initial condition for the velocity will change to

$$\dot{x}(0) = a\Omega' \exp(-\frac{\pi\Lambda'}{2\Omega'}). \tag{3.16}$$

As a result, the equation for the bead's position as a function of time changes to

$$x(t) = \frac{a\Omega'}{2\Lambda} \exp(-\frac{\pi\Lambda'}{2\Omega'}) (1 - \exp(-2\Lambda t)). \tag{3.17}$$

Since $x(t \to \infty) = d$, and using some algebra we arrive at

$$s' \exp(s') = \frac{\pi\alpha a}{4d}, \tag{3.18}$$

where s' is a dimensionless variable equal to $\frac{\pi\Lambda'}{2\Omega'}$.

The cantilever stiffness and the flexural rigidity will be found from the following equations:

$$\kappa = \frac{1}{3}kL^3 = \frac{9\pi\eta^2 L^3}{4\rho R} \left(\frac{\pi^2\alpha^2}{4[W\left(\frac{\pi\alpha a}{4d}\right)]^2} + \alpha^2 \right). \tag{3.19}$$

Again we have changed our variable from mass of the bead to its density in the last step. Note that the above formula for the cantilever stiffness and flexural rigidity (the second shooting-bead formula) for the case of α=1 reduces to the first shooting-bead formula (when the filament energy loss is not taken into account).

Figure 3.4 shows the effects of filament energy-loss consideration on the dimensionless flexural rigidity [11] curve as a function of a/d for three different filament radii, which corresponds to three different values of the filament energy-loss factor. To calculate the cantilever stiffness and the flexural rigidity for any other radius, first the filament energy-loss factor is calculated from Equation (3.9) and then this value is substituted into Equation (3.19). As is

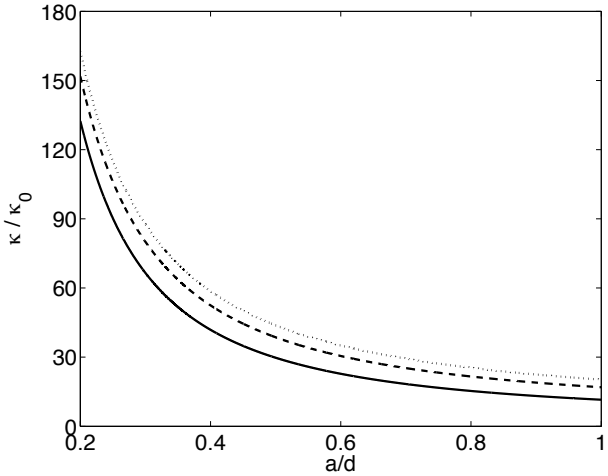

Figure 3.4 A plot of the dimensionless flexural rigidity κ/κ_0 as a function of a/d for a 10 μm filament and 1 μm bead diameter for three different situations: a) the solid curve, without filament energy loss consideration (which corresponds to the filament energy-loss factor of 1.0), b) the dashed curve for a 50 nm filament radius which corresponds to a filament energy-loss factor of 1.562, and c) the dotted curve for a 200 nm filament radius which corresponds to a filament energy-loss factor of 1.868.

clear from the graph for a single value of the ratio of a/d, the dimensionless flexural rigidity increases as a function of the filament energy loss factor. This is easy to understand since a higher fraction of the bending potential energy of the filament will be used to cancel out the energy-loss of the filament due to viscous drag torque.

Another important outcome that we can conclude from the effect due to the filament energy-loss factor on the dimensionless flexural rigidity curve is dependency of this effect on the ratio of a/d . Figure 3.5 shows the ratio of the flexural rigidity with consideration given to the filament energy-loss factor, κ', to the flexural rigidity without considering the filament energy-loss factor, κ,

as a function of a/d for the two previously considered filaments.

As we see from this graph, κ'/κ increases for any filament (with the inclusion of the filament energy-loss factor) when a/d increases. We also see from Figure 3.4 that when a/d increases for a filament with a known radius and length and also a known bead's radius (this means that we know the filament energy-loss factor), the dimensionless flexural rigidity decreases. This leads us to state the following important result: *Consideration of the filament energy-loss (or filament drag) is more important for filaments with less rigidity than for stiff ones.*

Since our answer is parametric and flexural rigidity depends on the values of, a/d, L, r, R, η, ρ we can end up with a wide range of values for flexural rigidity (note that the method works provided the bead passes through the origin, which means when we have underdamped motion for the bead) but we give a rough estimate of the flexural rigidity value based on our pilot experiment (not reported in this article due to its preliminary character). For an approximately 10 μm filament length, 100 nm filament radius (made from tubulin dimers, see the last section), 1 μm bead radius, immersed in an aqueous solution and also with $a = d = 1$ μm we end up with 10^{-17} for the order of magnitude in SI units of the flexural rigidity estimate. We expect that with different values for length and a/d the result may decrease by a few orders of magnitude. Therefore, our method is concluded to be most suitable for rigid filaments such as MT bundles, cilia and especially single-walled and multi-walled CNTs [13].

Stiff Filament Approximation

For stiff filaments we have a condition $\alpha a/d \ll 1$ and hence we can keep just the first term of the expansion of $s' \exp(s')$ in Equation (3.18). In that case, the filament's cantilever stiffness and flexural rigidity can be found from the following formula:

$$\kappa = \frac{1}{3} k L^3 = \frac{9\pi\eta^2 L^3}{\rho R} \left(\frac{d^2}{a^2}\right). \tag{3.20}$$

In the last step to reach Equation (3.20) we ignored $\alpha^2/4$ with respect to d^2/a^2 which directly follows from our approximation. Note that in the case of the stiff filament approximation there is no dependence on the filament energy-loss factor because in that case the area swept by the filament is very small (due to a small value of a with respect to d). This is also clear from Figure 3.5 when both curves approach unity at $a/d = 0$ regardless of the amount of filament energy-loss factor.

3.5 Sources of Error

In this section we wish to analyze the role of various sources of experimental error in the evaluation of the filament stiffness. To reach that goal, first we derive an equation for the percentage error for the first shooting-bead formula based on the error in our measurable quantities a and d (also η, ρ, L and R when calculating $\delta\kappa_0$). In the second part of this section we consider the effects of thermal diffusion and will demonstrate that using modern instruments these

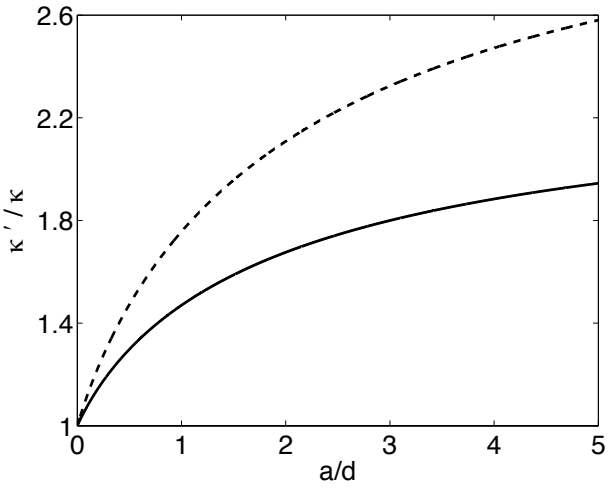

Figure 3.5 A plot of a ratio of the flexural rigidity with consideration of the filament energy-loss factor, κ', to flexural rigidity without consideration of the filament energy-loss factor, κ, as a function of a/d for two filaments considered in Figure 3.4: a) the solid curve for a 50 nm filament radius which corresponds to a filament energy-loss factor of 1.562 and b) the dashed curve for a 200 nm filament radius which corresponds to a filament energy-loss factor of 1.868.

effects are expected to be relatively small.

3.5.1 Error Calculation for the First Shooting-Bead Formula

Since it is our intention to derive an error formula for the most general case we perform error calculations for the dimensionless flexural rigidity. At the end, knowing the error of κ_0, we can calculate the final error for the flexural rigidity (see Appendix D for the calculation of $\delta\kappa_0$ and $\delta\kappa$). Taking the differential of Equation (3.4) gives

$$\delta(\frac{\kappa}{\kappa_0}) = \frac{\kappa}{\kappa_0}\frac{2\pi^2\delta W}{4W^3+\pi^2 W}, \tag{3.21}$$

but we know from Equation (3.18) that

$$\delta W = (\frac{\delta a}{a} + \frac{\delta d}{d})\frac{W}{1+W}. \tag{3.22}$$

Note also that as we are calculating the error for the first shooting-bead formula we should consider $\alpha = 1$ in order to get the above equation.

Substituting Equation (3.22) into Equation (3.21) we obtain

$$\delta(\frac{\kappa}{\kappa_0}) = \frac{\kappa}{\kappa_0}(\frac{\delta a}{a} + \frac{\delta d}{d})\frac{2\pi^2}{(1+W)(\pi^2+4W^2)}. \tag{3.23}$$

To calculate the percentage error in the measurement of dimensionless flexural rigidity, first we have to evaluate the last ratio in Equation (3.23). Figure 3.6 shows this ratio in Equation (3.23) as a function of a/d. Measuring a/d, we need to find the corresponding value for this ratio from this graph but to facilitate the use of the above formula, we notice that the last denominator

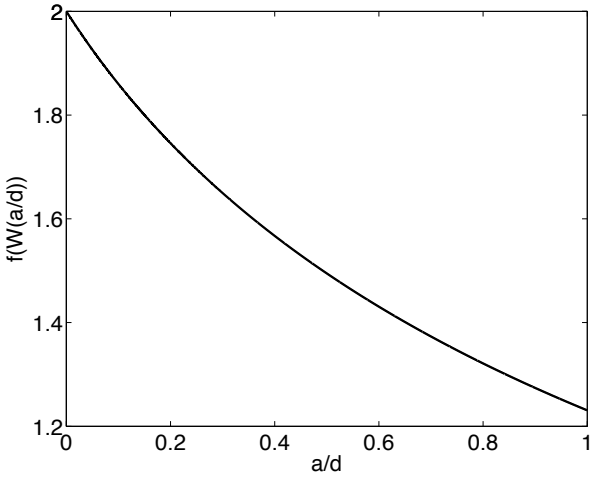

Figure 3.6 Plot of the last ratio in Equation (3.23), $f(W) = 2\pi^2/((1+W)(\pi^2+4W^2))$, as a function of a/d.

in Equation (3.23) is a monotonically increasing function on the entire domain of W which has its global minimum equal to π^2 at the beginning of the domain of W (at $W = 0$ which corresponds to $a/d = 0$). This means we can estimate an upper limit for the error calculation for the dimensionless flexural rigidity as

$$\delta(\frac{\kappa}{\kappa_0}) \leq \frac{\kappa}{\kappa_0} 2(\frac{\delta a}{a} + \frac{\delta d}{d}). \tag{3.24}$$

Measuring a and d and knowing the resolution of the instrument, we can estimate the upper limit for the percentage error for the dimensionless flexural rigidity from the above formula. To provide a rough estimate of the error in this method, we consider $a = d = 1$ μm (these are very close values to those seen in our preliminary experiment). With an accurate instrument it is possible to measure distances as small as 0.1 nm. Reference [19] provides some

information about high-resolution, single-molecule measurements. Here, we consider $\delta a = \delta d = 1$ nm to obtain a conservative estimate for the percentage error. Substituting the above values to Equation (3.24) we obtain 0.4% for the upper limit (the actual value found using Equation (3.23) or Figure 3.6 is 0.25%) of the percentage error for the dimensionless flexural rigidity.

3.5.2 Diffusion

For large beads, more than a 1 μm in radius, random thermal motion is not very pronounced (it has not been observed in our preliminary experiment) but we nevertheless wish to calculate the effects of thermal diffusion in a general case for this experiment in this section.

We know that[4] the diffusion constant for a spherical bead with radius R at temperature T is $k_B T/6\pi\eta R$. Also the relation between the mean square displacement, $(\Delta X)^2$ and time, t, involves the diffusion constant D as a proportionality constant [20], i.e., $(\Delta X)^2 = 2Dt$. Combining the two equations we obtain

$$(\Delta X)^2 = \frac{k_B T}{3\pi\eta R} t. \tag{3.25}$$

The elapsed time for the damped motion of the bead is on the order of asymptotic approach time constant, τ. For example, after a period of 9τ, the bead passes 99.988% of its final displacement (the number 9 has been used to simplify the answer), thus using the definition of τ and the above equation,

[4] Combining the Einstein relation, $D = k_B T/\gamma$, and Stokes' law, $\gamma = 6\pi\eta R$, we can easily get this equation. γ in previous equations represents the drag coefficient [9].

the root mean square of the displacement due to the diffusion can be found as

$$\Delta X = (\frac{2k_B T \rho R}{3\pi\eta^2})^{\frac{1}{2}}. \tag{3.26}$$

At $T = 25\ ^oC$, in an aqueous solution for a bead with 1 μm radius and a density equal to that of water we find ΔX=0.935 nm. This is a relatively small value which can serve as an approximate measure of the lower bound of the experimental error in the bead position for our calculation.

3.6 Discussion and Conclusion

In our preliminary experiment [21] some tubulin-based biotinylated bio- filaments have been produced due to the spontaneous aggregation of the tubulin dimers in the laboratory sample. Estimating the dimensions of the filaments observed in the solution (approximately 20-30 μm in length and 200 nm in width), we surmise that these semi-flexible objects were composed of microtubule bundles consisting of several or more microtubules in a bundle. While the diameter of a microtubule is 25 nm, the spatial resolution of the images was not sufficient to ascertain how far apart each microtubule was in a bundle. Since the images indicate splaying apart of bio-filaments at far ends of some of the bundles, we conclude that these were not individual macrotubes but several microtubules forming a bundle. During the experiment (when pushing the tip of a clamped bio-filament by a streptavidin coated bead to create an attachment point), we observed a strange effect involving a catapult-like release of the micro-bead from the filament and a subsequent projectile motion until it stopped following a very rapid movement through the solution. Seeing this

effect that can be described as a "jumping bead" phenomenon in the lab was the main motivation behind our effort to find a physical description reported in the present paper. While the experiment itself is still in progress, the method proposed here allows to us probe one of the important characteristics of stiff bio-filaments and nano-filaments with a very fast and relatively uncomplicated measurement of the initial and final position of the bead. Also, knowing precisely the cross-section of the filament and measuring the associated flexural rigidity, we are able to calculate the Young modulus of the filament.

In conclusion, we note that the method presented in this thesis offers numerous advantages over the other methods currently in use (e.g. the buckling force method [22, 23], the hydrodynamic flow method [24, 25], the wiggle and relaxation methods [26, 27], or the thermal fluctuation technique [28]) for the reasons listed below:

For this experiment, the bead need not be attached to the filament, actually, this was one of the reasons that guided the introduction of the proposed method. It needs just a single trap, there is no need to find the force exerted on the bead by the trap, there is no need to know the exact shape of the filament, there is no need to oscillate the trap, there is no need to measure the time and there is no need to measure the velocity of the bead or the rod. The only measurement that we need to perform is the measurement of the length for a and d, also because the ratio of a/d is important not a and d individually, there is no need to calibrate the microscope.

Another aspect that we should briefly discuss here is the logarithmic dependence of the viscous drag torque exerted on the filament on the radius and length of the filament. Even for a thin filament it is important to consider the effects of filament energy-loss factor on the dimensionless flexural rigidity

curve. Figure 3.3 shows that even for small values of the filament radius, the filament energy-loss factor is not very close to one. This is also clear from Figure 3.4, as we see the dimensionless flexural rigidity curve for the filament with a 50 nm radius (the dashed curve) is much closer to the dimensionless flexural rigidity curve for the filament with a 200 nm radius (the dotted curve) compared with the curve without filament energy loss consideration (the solid curve).

Also dependence of the dimensionless flexural rigidity on the length of the filament via the filament energy-loss factor is very important. Even for a small radius of the filament compared to the bead's radius, if we increase L, L varies much faster than $\ln(L)$ in Equation (3.9). Therefore, α will have a considerable value.

Ultimately we demonstrated that the effect due to the filament energy-loss factor on the dimensionless flexural rigidity curve increases as a/d increases. As we know, when this ratio increases for a filament with a known radius and length and also a known radius of the bead, the (dimensionless) flexural rigidity decreases. This means consideration of the filament energy-loss (or filament drag) is more important for filaments with less rigidity.

Since MTs exhibit mechanoelastic properties of considerable interest in view of their functional roles in cell division and cell shape, In the next chapter we discuss the effect of ultrasound plane wave on the microtubules with solving the related beam equation for it.

Bibliography

[1] E. Unger, K. Boehm, and W. Vater, Electron Microsc. Rev. 3, 355-395 (1990).

[2] P.A. Janmey, U. Euteneuer, P. Traub, and M. Schliwa, J. Cell Biol. 113, 155 (1991).

[3] L. Ma, J. Xu, P.A. Coulombe, and D. Wirtz, J. Biol. Chem. 274, 19145 (1999).

[4] D. Boal, Mechanics of the cell, Cambridge University Press, Cambridge, (2002).

[5] P. Meurer-Grob, J. Kasparian, and R. H. Wade, Biochemistry 40, 8000 (2001).

[6] A. Kis, S. Kasas, B. Babic, A. J. Kulik, W. Benoit, G. A. D. Briggs, C. Schonenberger, S. Catsicas, and L. Forro, Phys. Rev. Lett. 89, 248101 (2002).

[7] J. A. Tuszynski, T. Luchko, S. Portet, and J. M. Dixon, Eur. Phys. J. E 17, 29-35 (2005).

[8] S. Portet, J. A. Tuszynski, C. M. Hogue, and J. M. Dixon, Eur Biophys. J. 34, Number 7, 912-920 (2005).

[9] J. Howard, Mechanics of Motor Proteins and the Cytoskeleton, Sinauer Associates Inc., Sunderland, Massachusetts (2001).

[10] O. Lieleg, M. M. A. E. Claessens, C. Heussinger, E. Frey, and A. R. Bausch, Phys. Rev. Lett. 99, 088102 (2007).

[11] A. Samarbakhsh and J. A. Tuszynski, J. Comput. Theor. Nanosci. 5, 2041-2044 (2008).

[12] K. M. Taute, F. Pampaloni, E. Frey, and E.-L. Florin, Phys. Rev. Lett. 100, 028102 (2008).

[13] C. Ni, C. Deck, K. S. Vecchio, and P. R. Bandaru, Appl. Phys. Lett. 92, 173106 (2008).

[14] K. C. Neuman and S. M. Block, Rev. Sci. Instrum. 75, 2787-2809 (2004).

[15] K. T. McDonald, Am. J. Phys. 68, 486-488 (2000).

[16] J. B. Marion, Classical Dynamics of Particles and Systems, 2nd ed., Academic Press Inc., New York, New York (1970).

[17] L. A. Segel, Mathematics Applied to Continuum Mechanics, Dover Publications Inc, New York (1987).

[18] Corless, R. M.; Gonnet, G. H.; Hare, D. E. G.; Jeffrey, D. J., and Knuth, D. E, Adv. Comput. Math. 5, 329-359 (1996).

[19] W. J. Greenleaf, M. T. Woodside, and S. M. Block, Annu. Rev. Biomol. Structure 36, 171-190 (2007).

[20] G. B. Benedek, F. M.H. Villars, Physics With Illustrative Examples From Medicine and Biology (Statistical Physics), 2nd ed., Springer-Verlag New York Inc, New York (2000).

[21] L. Payet (private communication).

[22] M. Kikumoto, M. Kurachi, V. Tosa, and H. Tashiro, Biophysical Journal, 90, 1687-1696 (2006).

[23] M. Kurachi, M. Hoshi, and H. Tashiro, Cell Motil. Cytoskeleton 30, 221-228 (1995).

[24] P. Venier, A. C. Maggs, M.-F. Carlier, and D. Pantaloni, J. Biol. Chem. 269, 13353-13360 (1994).

[25] J. C. Kurz, and R. C. Williams, Jr., Biochemistry. 34, 13374-13380 (1995).

[26] H. Felgner, R. Frank, and M. Schliwa, J. Cell Sci. 109, 509-516 (1996).

[27] H. Felgner, R. Frank, J. Biernat, E.-M. Mandelkow, E. Mandelkow, B. Ludin, A. Matus, and M. Schliwa, J. Cell Biol. 138, 1067-1075 (1997).

[28] F. Gittes, B. Mickey, J. Nettleton, and J. Howard, J. Cell Biol. 120, 923-934 (1993).

[29] J. M. Gere and S. P. Timoshenko, Mechanics of Materials, 3rd SI ed., Chapman and Hall, London (1991).

Chapter 4

Resonance Condition in Microtubules Using Ultrasound Plane Waves*

4.1 Introduction

Ultrasound has been successfully used in medical imaging and it is widely accepted today that High Intensity Focalized Ultrasound (HIFU) may provide an effective non-invasive targeted modality that could help to deliver drugs in cells or else become an alternative to surgery in the treatment of both benign and malignant diseases. Kennedy et al. [1] summarized the potential use of this technique as a surgery from clinical trial data. For example, it was shown that HIFU was successful in reducing tumor size and pain and showed no adverse side effects for patients with pancreatic cancer [2]. The efficiency of this

*A version of this chapter has been submitted for publication.

technique was shown to depend on physical parameters such as the frequency, the intensity, the duration of the pulses and time interval between pulses. For medical trials, the frequency ranges between 0.8 and 1.7 MHz and the intensity 1 and 20 KW/cm^2 were used. However, further studies are necessary to understand the therapeutic mechanism of HIFU, to optimize the delivery of HIFU to the tumor site and decrease potential side effects. To understand the action of HIFU on cell structure, most studies thus far have been performed on either cultured or isolated cells [3, 4]. In their studies on isolated cells, Hrazdira et al. [4] have shown the partial disassembly of all components of the cytoskeleton and particularly microtubules as a result of ultrasound exposure. In addition, it appears that the effects of ultrasound depend on the phase of the cell cycle during which the exposure takes place [4], with mitosis being the most sensitive phase. This disassembly was characterized by thinning of fibrous structures, their fragmentation and formation of granule-like structures. However, it is difficult to precisely interpret their experiments because when the experiment was performed on cells, other constituents of the cell were not properly monitored and analyzed (e.g. actin filaments). Therefore, it is necessary to study first of all isolated microtubules and their behaviour under the influence of externally applied ultrasound. Interestingly, these authors observed that ultrasound of intensities as low as 100 mW/cm^2 with a frequency of 0.8 MHz is enough to induce these damages. All these studies showed that, depending on the physical parameters cited above, ultrasound damages or destroys cancer cells through three predominant mechanisms: heating, cavitation (repeated mechanical shocks intensified by formation of microbubbles) [1], and most interestingly mechanical shocks that break rigid filaments such as microtubules without heating and cavitation.

Since microtubules play a crucial role in cell division and since they have been shown to be strongly affected by ultrasound effects, in this study, we aimed to study theoretically the mechanics of microtubules in the absence of other cellular constituents and their behavior under the influence of externally applied ultrasound in situations where both cavitation and heating are negligible. In particular, we are interested in determining the existence of mechanical resonance conditions in terms of frequency, mode of application and the energy needed to eventually break microtubules since they play such an important role in the mitosis process. The study of ultrasound effects on isolated microtubules is necessary to help understand its basic mechanisms of action on cells and tissues and it is a fundamental question in nanophysics. Our ultimate goal is to improve the design and hence the use of HIFU for the treatment of cancer using non-invasive techniques. Recently, novel ultrasonic techniques, such as the acoustic lens [5], have been developed which offer additional capabilities of being able to focus the acoustic energy at specific locations. This if properly fine tuned can lead to oncologic applications of relevance to the research presented in this chapter.

4.2 Theory and Calculation

In this section we will analytically solve the MT equation under the influence of an ultrasound plane wave. Our primary aim is to solve the problem analytical and general for different filaments. To do that we use the the so called beam equation [6, 7] or filament equation in this section. At section 4.4, with the parametric solution that will be found in this and next sections,

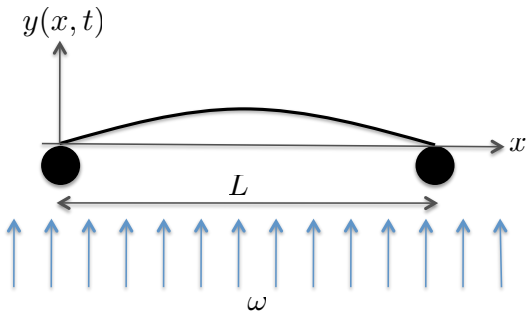

Figure 4.1 Schematic illustration of a microtubule that is attached to two beads at its ends that can be considered as situation of the MT during mitosis

we will substitute the related values for the MT and will find the result for MT. The parametric analytical solution also will help the other researchers to use the solution with substituting the parameters for their correspondence filament. Here, first we calculate the solution of free vibration of the MT and then we will find the response of MT vibration when it is driven by an ultrasound source with different frequencies when the microtubule is simply attached at its two ends which is very good representation of the microtubule during mitosis.

Fig. 4.1 shows a schematic drawing of a microtubule with length L that is simply pinned at its two ends by attaching it to the two beads that are trapped by laser tweezers [8,9] that can be considered as a microtubule during mitosis.

The equation of motion of the filament, driven with a sinusoidal force density (force per unit of length of the beam) with amplitude of EIA^1 and

angular frequency of ω is

$$\frac{\partial^4 y(x,t)}{\partial x^4} + \frac{c_\perp}{EI}\frac{\partial y(x,t)}{\partial t} + \frac{\mu}{EI}\frac{\partial^2 y(x,t)}{\partial t^2} = A\sin(\omega t). \tag{4.1}$$

The second and the third terms on the left side of the above equation come from the viscous drag force of the solution and the inertia of the beam respectively and the term on the right side represents the effect of the ultrasound source. Also in Eq. (4.1) the viscous drag coefficient per unit of the length of the filament, flexural rigidity of the filament, and the linear mass density of the filament are denoted as $c_\perp$, EI, and μ respectively.

4.2.1 Complementary solution or Free Vibration Solution

To solve the above equation, first we will find the solution for the homogeneous equation. By setting the right hand side of Eq. (4.1) equal to zero (to get the complementary function) and assuming that the solution for $y(x,t)$ is a separable function of x and t we write

$$y(x,t) = X(x)Y(t). \tag{4.2}$$

Substituting Eq. (4.2) into Eq. (4.1) and dividing the result by $X(x)Y(t)$,

[1] This amplitude is always proportional to the amplitude of the ultrasound at the location of the MT, which is related to the intensity of the wave at the location of the MT. In this section we are not interested in calculating this quantity since our solutions are always proportional to A and we always have a good control of it through the intensity of the wave. We will come back to this issue in Section 4.6.

we get the following two eigenvalue equations

$$\frac{d^4X(x)}{dx^4} = \alpha X(x), \tag{4.3}$$

$$\frac{d^2Y(t)}{dt^2} + \frac{c_\perp}{\mu}\frac{dY(t)}{dt} = -\alpha\frac{EI}{\mu}Y(t). \tag{4.4}$$

α is an arbitrary constant at this stage. As we mentioned before, we solve the equation for a MT that has been simply attached at its two ends, that means the boundary conditions for Eq. (4.3) are

$$X(0) = X(L) = 0, \qquad \frac{d^2X}{dx^2}\mid_{x=0} = \frac{d^2X}{dx^2}\mid_{x=L} = 0. \tag{4.5}$$

Applying the above boundary conditions in Eq. (4.3), we will get the eigenfunctions and eigenvalues of Eq. (4.3) as

$$X_n(x) = \sin(\alpha_n^{1/4}x), \qquad \alpha_n = (\frac{n\pi}{L})^4. \tag{4.6}$$

Time dependency of the solution depends on mode number, n, of the solution. It can give us two different situations[2] based on our mode number:

1) Overdamped case $\alpha_n\frac{EI}{\mu} < (\frac{c_\perp}{2\mu})^2$

2) Underdamped case $\alpha_n\frac{EI}{\mu} > (\frac{c_\perp}{2\mu})^2$

The time solution will be

[2]In fact it gives 3 different situations and here we have assumed that $\alpha_n EI/\mu \neq (c_\perp/2\mu)^2$. In the case of the critically damped solution, $\alpha_n EI/\mu = (c_\perp/2\mu)^2$, we have to add another term to our solution in Eq. (4.8).

$$Y_{c_n}(t) = \begin{cases} \exp(-\frac{c_\perp}{2\mu}t)[A_n \exp(\sqrt{(\frac{c_\perp}{2\mu})^2 - \alpha_n \frac{EI}{\mu}}t) \\ \qquad\qquad + B_n \exp(-\sqrt{(\frac{c_\perp}{2\mu})^2 - \alpha_n \frac{EI}{\mu}}t)], & n \leq n_c \\ C_n \exp(-\frac{c_\perp}{2\mu}t)\cos(\sqrt{\alpha_n \frac{EI}{\mu} - (\frac{c_\perp}{2\mu})^2}t - \delta_n), & n > n_c \end{cases} \tag{4.7}$$

where $n_c = \lfloor \frac{L}{\pi}(\frac{\mu}{EI})^{1/4}(\frac{c_\perp}{2\mu})^{1/2} \rfloor$ is the integral part[3] of $\frac{L}{\pi}(\frac{\mu}{EI})^{1/4}(\frac{c_\perp}{2\mu})^{1/2}$ and A_n, B_n, C_n, and δ_n can be found from the initial condition of the beam.

Thus with using Eq. (4.6) for the spatial part and Eq. (4.7) for the temporal part of the function we can write the following equation for the solution of the homogeneous part of the beam equation,

$$y_c(x,t) = \sum_{n=1}^{\infty} y_{c_n}(x,t) = \sum_{n=1}^{\infty} X_n(x) Y_{c_n}(t). \tag{4.8}$$

4.2.2 Particular Solution for a Microtubule Driven by a Sinusoidal Plane Wave

In this section we will solve the beam equation for microtubule that is driven with a sinusoidal ultra-sound wave. To do that, we first look for a particular solution of Eq. (4.1). Unfortunately we can not find this particular solution with the method of separation of variables directly, because the driven part does not have spatial dependency. Therefore, we assume that our driven force is $AX(x)\sin(\omega t)$, instead of $A\sin(\omega t)$ at our first attempt to find a particular solution. This will help us to solve our differential equation with

[3]It is also called integral value or floor function (usually in mathematics). In mathematics and computer science, the floor functions map a real number to the next smallest integer. More precisely, floor(x) is the largest integer not greater than x.

the method of separation of variables. Later in this section we will talk about the logical reasons to accepting this assumption and showing that this is not a limitation for the method of solution.

Substituting Eq. (4.2) into Eq. (4.1) with the new driven force and dividing the result to $X(x)Y(t)$ we will again get two eigenvalue equations. The eigenvalue equation related to the spatial part is the same as Eq. (4.3) and eigenvalue equation related to the temporal part will be

$$\frac{d^2Y(t)}{dt^2} + \frac{c_\perp}{\mu}\frac{dY(t)}{dt} + \alpha\frac{EI}{\mu}Y(t) = \frac{EIA}{\mu}\sin(\omega t). \tag{4.9}$$

Again applying the initial conditions mentioned in Eq. (4.5), in Eq. (4.3), we will get the the same eigenfunctions and eigenvalues as in Eq. (4.6). For the temporal function we try [10] $D\sin(\omega t - \delta)$ as a particular solution. Putting this function in the Equation (4.9) and expanding $\sin(\omega t - \delta)$ and $\cos(\omega t - \delta)$ and using the fact that $\sin\omega t$ and $\cos\omega t$ are linearly independent we can find D and δ and consequently our particular solution will be

$$Y(t) = \frac{\frac{EIA}{\mu}}{[(\alpha\frac{EI}{\mu} - \omega^2)^2 + 4(\frac{c_\perp}{2\mu})^2\omega^2]^{1/2}}\sin(\omega t - \delta), \tag{4.10}$$

where δ in Eq. (4.10) is

$$\delta = \tan^{-1}(\frac{\frac{c_\perp}{\mu}\omega}{\alpha\frac{EI}{\mu} - \omega^2}). \tag{4.11}$$

This is the particular solution for the temporal part of our microtubule equation that represents all of the information for large[4] t. Using Eq. (4.6) for the spatial function and Eq. (4.10) for the temporal function we can find the complete particular solution for the microtubule vibration,

$$y_p(x,t) = \sum_{n=1}^{\infty} y_{p_n}(x,t) = \sum_{n=1}^{\infty} B_n X_n(x) Y_{p_n}(t)$$
$$= \sum_{n=1}^{\infty} B_n \sin(\alpha_n^{1/4} x) \frac{\frac{EIA}{\mu}}{[(\alpha_n \frac{EI}{\mu} - \omega^2)^2 + 4(\frac{c_\perp}{2\mu})^2 \omega^2]^{1/2}} \sin(\omega t - \delta_n). \quad (4.12)$$

Note that α_n has been calculated in Eq. (4.6). B_n can be found from the space dependency of the driven force.

Now we come back to the assumption that we did to be able to use method of separation of variables and we found the particular solution for the non homogeneous term of $AX(x)\sin(\omega t)$ instead of $A\sin(\omega t)$. As we know the eigenfunctions of Eq. (4.3), $X_n(x)$, produce a complete (or closed) set over the domain of]0,L[which means that we can expand any spatial function for the right hand side of Eq. (4.1) in terms of a linear combinations of these eigenfunctions. Since our beam equation is also linear, the particular solution for any spatial function in the driven part will be a linear combination of solutions in Eq. (4.12) with the same coefficient B_n.

To find B_n for the original problem, when the the non homogeneous term is $A\sin(\omega t)$, we just need to expand one over the domain of]0,L[in terms of eigenfunctions $X_n(x)$. With doing that we get [11] (Appendix E)

$$1 = \frac{4}{\pi}[\frac{\sin(\pi x/L)}{1} + \frac{\sin(3\pi x/L)}{3} + \frac{\sin(5\pi x/L)}{5} + ...]. \quad (4.13)$$

Using the coefficients in the above expansion and substituting them into Eq. (4.12) and simplifying the result, we will get the following exact particular solution for the MT equation with non homogeneous term of $A\sin(\omega t)$,

[4]Here "large" means compare to the inverse of damping parameter, $c_\perp/2\mu$, in the complementary solution in Eq. (4.7). It means for $t \gg 2\mu/c_\perp$ our solution can be demonstrated just by the particular solution.

$$y_p(x,t) = \sum_{n=1,\ odd}^{\infty} \frac{4A}{n\pi[(n^4(\frac{\pi}{L})^4 - \frac{\mu}{EI}\omega^2)^2 + (\frac{c_\perp}{EI})^2\omega^2]^{1/2}} \sin(n\pi x/L)\sin(\omega t - \delta_n). \tag{4.14}$$

Now that we have found the exact particular solution for the microtubule equation driven by an ultrasound plain wave and we know that this term(s), particular solution, is the only important term(s) just after a few oscillations of the microtubule, we are ready to evaluate any quantity that we are interested in.

4.3 Maximum Bending and Resonance Condition

In this section first we will calculate the bending moment exerted on the cross section of the microtubule. The reason for this calculation is that the bending moment is the quantity responsible for bending any beam or filament and if it exceeds some critical value (for a given filament with a cross section and material), the filament will break. Using the moment-curvature relationship, $M = EI/\rho$, [12] and using the small deflection approximation, $1/\rho = \partial^2 y(x,t)/\partial x^2$, we can find the bending moment with taking the partial derivative of particular solution with respect to the x,

$$M(x,t) = \sum_{n=1,\ odd}^{\infty} \frac{-4(\frac{n\pi}{L})^2 EIA}{n\pi[(n^4(\frac{\pi}{L})^4 - \frac{\mu}{EI}\omega^2)^2 + (\frac{c_\perp}{EI})^2\omega^2]^{1/2}} \sin(n\pi x/L)\sin(\omega t - \delta_n). \tag{4.15}$$

Then we are looking for the frequencies that maximize the bending moment for each mode. To do that, we should maximize the amplitudes of the bending moment with respect to the frequency. Taking a derivative of the amplitudes of the bending moment in Eq. (4.15) with respect to ω and setting them to zero, introduces the frequencies that we are seeking. The frequencies are

$$\omega_n = [(\frac{n\pi}{L})^4 \frac{EI}{\mu} - 2(\frac{c_\perp}{2\mu})^2]^{1/2}. \tag{4.16}$$

Note that in the above equation resonance just happens for the values of n that make the quantity under the square root positive. Solving the above equation for the the smallest integer value of n that can give us the real value for the frequency, n_0, we will find the first resonance mode number as[5]

$$n_0 = \lceil \frac{L}{\pi} (\frac{\mu}{2EI})^{1/4} (\frac{c_\perp}{\mu})^{1/2} \rceil. \tag{4.17}$$

The reason for calling the above frequencies as resonance frequencies is that they are exactly the same frequencies that maximize the amplitudes in MT equation (Eq. (4.14)) and we know that when the amplitude in the MT equation is maximum for each frequency the correspondent mode absorbs the maximum amount of the energy from the source. In fact this is the definition of resonance frequency.

[5] "$\lceil\rceil$" in Eq. (4.17) is called celling function that maps the argument to the next largest integer. Also note that in this section n can just accept odd numbers and if we end up with an even number for n_0 in Eq. (4.17), we should go to the next integer which is definitely an odd number.

4.4 Analytical Results

In this section we substitute physical values for the parameters in our solution. Fig. 4.2a (left axis) shows the graph of the resonance frequency as a function of mode number for a MT with a length of 10 μm that is inside an aqueous solution. Viscosity of the solution is 10^{-3} Pa.s [13] and the diameter and flexural rigidity of MT are equal to 25 nm and 3×10^{-23} Nm^2 respectively [14, 15]. We also need to calculate $c_\perp$ from the following equation [13, 16]:

$$F_\perp = \frac{4\pi\eta L}{\ln(\frac{L}{2r}) + 0.84}\, v, \tag{4.18}$$

where $F_\perp$ is the perpendicular component of the viscous force exerted on the MT by the solution when it moves with velocity v with respect to the solution. η is viscosity of the solution and L and r are length and radius of the filament respectively.

As we see from the graph, the first resonance happens at mode number equal to 67 and before that mode there is no resonance and the amplitude of the bending moment decreases as a function of frequency monotonically.

Fig. 4.3 shows the amplitude of the bending moment (actually it shows the amplitude of the bending moment divided by EIA, but as we explained in footnote 1, here we are just interested in maximizing the amplitude of the bending moment for a constant A which is always related to the intensity of the ultrasound at the location of the MT) at each resonance frequency as a function of mode number. As it is clear from the graph the amplitude decreases with increasing the mode number, this suggests that using the first mode of the resonance transfers the maximum amount of the energy to the MT compare

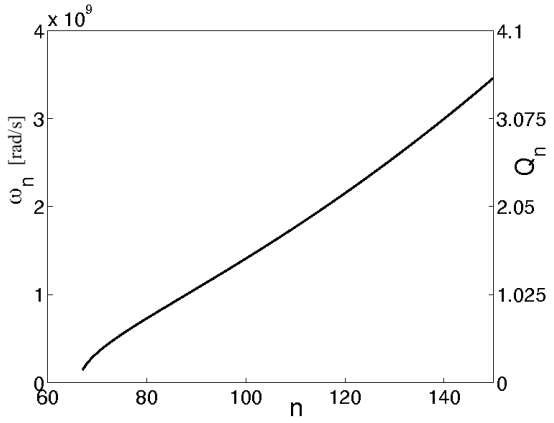

Figure 4.2 Left axis, Fig. 4.2a, shows a plot of the resonance frequency as a function of mode number for a 10 μm length microtubule inside the aqueous solution. Right axis, Fig. 4.2b, shows a plot of the quality factor of resonance as a function of mode number for the same microtubule.

with other resonance modes. We will come back to this statement later on when we discuss the quality factor of each mode.

Fig. 4.4 shows the amplitudes of the bending moment as a function of frequency for three different modes. As we see, the amplitude at the resonance frequency for the modes, maximum of the curves, decreases with increasing the mode number. This is also clear from Fig. 4.3 but here we want to bring the readers attention to this fact that although the amplitude at the resonance frequency decreases with increasing the mode number, the width of curves decreases faster in such a way that *Quality factor* (Q-factor) of the resonance that describes how underdamped an oscillator or resonator is, or equivalently describes the sharpness of each resonance (here Q-factor is equal to $\mu\omega_n/c_\perp$), increases with increasing the mode number. Unlike for the amplitude that suggests to use the first resonance mode for transferring the maximum amount

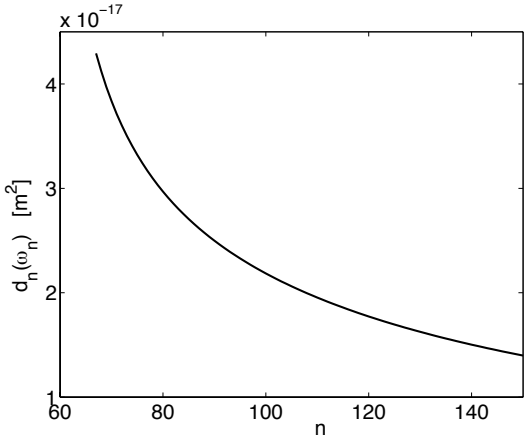

Figure 4.3 A plot of amplitude of the bending moment divided by EIA at each resonance frequency as a function of mode number for a 10 μm length microtubule inside the aqueous solution. In the above graph $d_n(\omega)$ is equal to $D_n(\omega)/EIA = 4(\frac{n\pi}{L})^2/n\pi[(n^4(\frac{\pi}{L})^4 - \frac{\mu}{EI}\omega^2)^2 + (\frac{c_\perp}{EI})^2\omega^2]^{1/2}$ and in order to get the above graph, we should substitute ω_n from Eq. (4.16) in the $d_n(\omega)$.

of the energy to the MT, Q-factor suggests that for having sharper resonance we should use modes with higher mode number. We will resolve this issue later with introducing the double slit ultrasound waves. Fig. 4.2b (right axis) shows the quality factor as a function of mode number.

Although we have solved and discussed the resonance condition, amplitude of bending moment at each resonance frequencies, and Q-factor of each mode, we should note that when the MT is driven by an ultrasound plane wave, the solution will be a linear combination of all modes in Eq. (4.15). More specifically when we discussed the resonance frequency for one specific mode, we really meant that the contributation of that mode when the filament is driven by a specific frequency is a maximum compared to its contribution when the filament is driven by any other frequencies. However, the MT actually

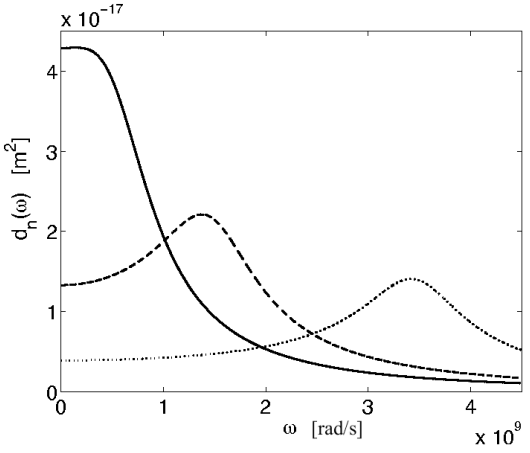

Figure 4.4 A plot of the amplitudes of the bending moment divided by EIA for a 10 μm length microtubule inside the aqueous solution as a function of the frequency for three different modes: (a) the solid curve for mode number equal to 67 (which corresponds to the first resonance mode, n_0), (b) the dashed curve for mode number equal to 99, and (c) the dotted curve for mode number equal to 149.

vibrates with a combination of all of its modes. Some of the modes with a lower, although not satisfying the resonance condition, have a larger amplitude than the amplitude of the specific mode.

Fig. 4.5 clearly demonstrates the previous paragraph. Although the mode number 99 is at resonance (solid curve at its peak), amplitudes of the mode number 97 (dashed curve) and 95 (dotted curve) are still higher than the amplitude of this mode at its resonance frequency. This proves that the ultrasound plane waves really do not establish any resonance condition for the MT.

4.5 Single Mode Excitation

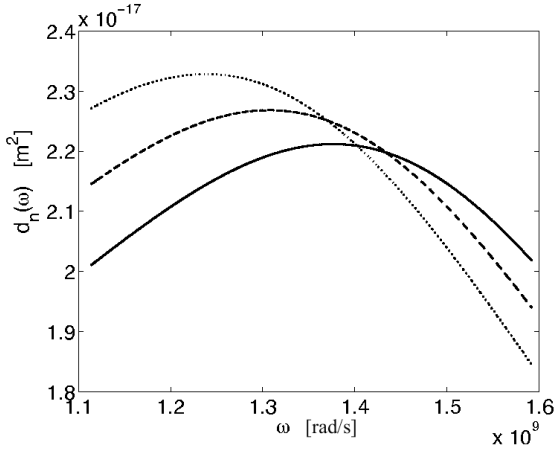

Figure 4.5 A plot of the amplitudes of the bending moment divided by EIA for the same microtubule as a function of the frequency for three consecutive modes: (a) the solid curve for mode number equal to 99, (b) the dashed curve for mode number equal to 97, and (c) the dotted curve for mode number equal to 95.

In order to control the system with frequency, we have to excite just one single mode with a mode number larger that n_0 (in order to have resonance) and eliminate the other modes. To do that we can no longer excite the filament with an ultrasound plane wave as mentioned before and we have to modulate our wave. Looking carefully to the steps we passed to reach the solution in Eq. (4.14), helps us to find out what kind of modulation we should have. For eliminating the other modes and exciting only a single mode[6], say m, we should eliminate the other terms in the summation in Eq. (4.15), but we know that the summation has come from the expansion of one in terms of $\sin(n\pi x/L)$ (in order to produce the plane wave). This explains why we cannot excite the filament with the plane wave anymore and guides us to excite the filament with a force density of the form of $EIA\sin(m\pi x/L)\sin(\omega t)$ instead of $EIA\sin(\omega t)$.

[6] In this chapter, we use m as a mode number when we excite a single mode with elimi-

Using the above force density, the solution for the MT vibrational equation and the bending moment equation can be found from the following equations respectively,

$$y_p(x,t) = \frac{A}{[(m^4(\frac{\pi}{L})^4 - \frac{\mu}{EI}\omega^2)^2 + (\frac{c_\perp}{EI})^2\omega^2]^{1/2}} \sin(m\pi x/L)\sin(\omega t - \delta_m), \quad (4.19)$$

$$M(x,t) = \frac{-(\frac{m\pi}{L})^2 EIA}{[(m^4(\frac{\pi}{L})^4 - \frac{\mu}{EI}\omega^2)^2 + (\frac{c_\perp}{EI})^2\omega^2]^{1/2}} \sin(m\pi x/L)\sin(\omega t - \delta_m). \quad (4.20)$$

In Fig. 4.6, we have shown a plot of the amplitudes of bending moment divided by EIA for a 10 μm length MT inside an aqueous solution. Comparing this figure with Fig. 4.4 reveals two major advantages of excitation of a single mode of the filament with the modulated wave of $EIA\sin(m\pi x/L)\sin(\omega t)$ with respect to excitation with the plane wave. First the amplitude is much larger in Fig. 4.6 (in fact it is $m\pi/4$ times larger since we do not need to expand the plane wave in terms of the harmonic modes). The second advantage is that with increasing the mode number, m, the amount of the amplitude of the bending moment at the resonance frequency (maximum of each graph) does not drop as fast as Fig. 4.4 and becomes almost flat for large mode number.

This is more clear in Fig. 4.7 which shows a plot of the amplitude of the bending moments divided by EIA at each resonance frequency as a function of mode number for the same filament for both kind of excitations. As we see, not only the modulated excitation gives us a much larger amplitude but also the amount of amplitude for large mode number is almost independent of the mode

nating the other modes (refere to Eq. (4.19) and (4.20)). n has been used for demonstration of mode number for excitation of a single mode by an ultrasound plane wave (refer to Eq. (4.14) and (4.15)).

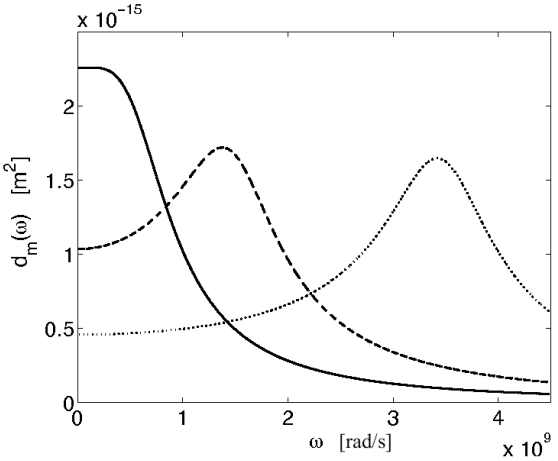

Figure 4.6 A plot of the amplitudes of bending moment divided by EIA for a 10 μm length microtubule when we have just excited a single mode at a time as a function of the frequency, for three modes: (a) the solid curve for $m = 67$, (b) the dashed curve for $m = 99$, and (c) the dotted curve for mode number equal to $m = 149$. Note that there is no need to pick the odd mode number when we excite just a single mode and eliminate the other modes but here we picked the same mode number demonstrated in Fig. 4.4 in order to be able to compare two situations accurately. Also note that unlike Fig. 4.4 that we have all the curve at any driven frequency (since we had excited the filament with a plane wave), here we have just excited a single mode of the system at a time with a driven force dencity of the form $EIA\sin(m\pi x/L)\sin(\omega t)$ and we should not consider the other curves.

number. The graph for Q-factor as a mode number remain exactly the same as excitation with the plane wave in Fig. 4.2b. As with modulated excitation we do not have the problem of dropping of the amount of the amplitude with increasing the mode number, these two graphs (Fig. 4.2b and Fig. 4.7) suggest that for having more control on the system, we should use higher mode numbers.

All of the above results guide us to excite just a single mode of the MT with a modulated wave of the form of $\sin(m\pi x/L)\sin(\omega t)$.

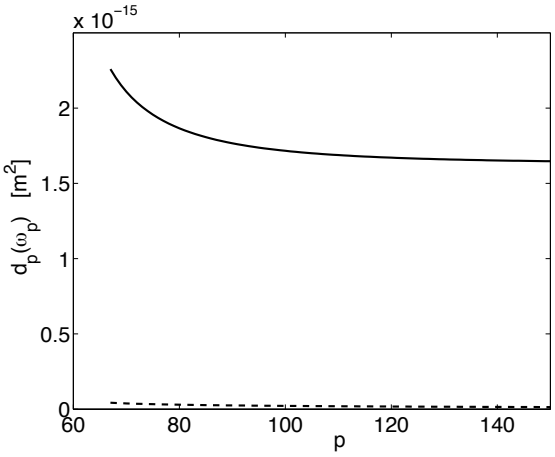

Figure 4.7 A plot of amplitude of the bending moment at each resonance frequency divided by EIA as a function of the mode number for a 10 μm length microtubule inside the aqueous solution. The solid curve (replacing p with m) shows excitation with modulated wave of $EIA\sin(m\pi x/L)\sin(\omega t)$. The dashed curve (replacing p with n) shows excitation with a plane wave with the same amplitude.

From the theoretical point of view the job is done and we have proved that in order to have frequency control on the vibration of the filament we should excite just one single mode of the filament but the experimental issue is how can we do that? Is there any device to produce such a modulated wave?

Although we do not intend to overcome all experimental issues and prefer to leave the answers to the above questions to the experimentalist but still try to open a direction for answering those questions. We think the answers are interference and double slit. With passing an ultrasound plane wave through a double slit we can produce the wave we are looking for. Fig. 4.8 shows a schematic.

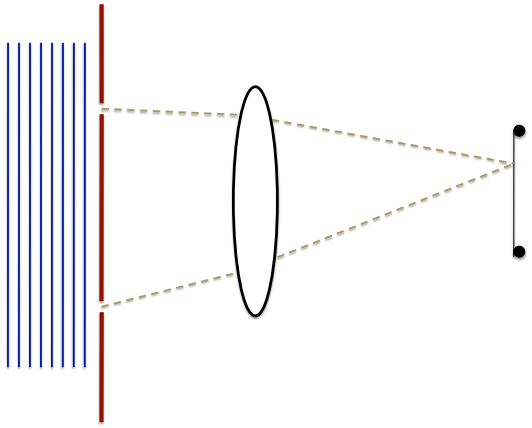

Figure 4.8 A schematic of proposed double slit ultrasound device for a single mode excitation. (Figure not to scale)

4.6 Intensity and Sound Level Estimation

In this section we try to calculate the minimum requirement on the ultrasound intensity to break a MT. In order to break a MT, we should bend it to a minimum local curvature. Reference [17] provides useful information about the breakage of MTs. The mean curvature to break a MT in Waterman-Storer's and Salmon's [18] report is around 1.7 rad/μm. Later, Odde et al. [17] reported 1.5 rad/μm for the related mean curvature. Substituting this reported curvature and flexural rigidity of a MT into the moment-curvature relationship, we can calculate the *minimum required bending moment* exerted on the cross section of a MT to break it. This value is about 4.5×10^{-17} Nm and is denoted by M_B in the rest of this section. Note that we should equalize M_B with the maximum of the bending moment in equation Eq. (4.20), which is simply the amplitude of the bending moment in that equation, to find the relation between M_B and the *minimum required ultrasound intensity* (denoted

by I_B in the rest of this section). This will be demonstrated later in this section. Also, as the maximum bending moment corresponds to the maximum of MT solution, Eq. (4.19), we can conclude that the breakage of MT happens at the locations of antinodes.

As we mentioned in section 4.2, EIA is the amplitude of the force density. This quantity is related to the *pressure amplitude* of ultrasound through the simple relation between the force and pressure,

$$EIA = 2r\Delta p_0, \tag{4.21}$$

where Δp_0 and r denote the pressure amplitude, which is the maximum increase or decrease in pressure due to ultrasound, and the radius of MT, respectively. Pressure amplitude is related to the *displacement amplitude*, which is the maximum displacement of the fluid element to either side of its equilibrium position, through the following formula [19]:

$$\Delta p_0 = v\rho_s\omega s_0, \tag{4.22}$$

where v, ρ_s, ω, and s_0 denote the speed of sound in the solution [20], density of the solution, angular frequency of ultrasound, and displacement amplitude, respectively. By eliminating Δp_0 between Eq. (4.21) and Eq. (4.22), then solving for s_m, we obtain the following equation for the displacement amplitude,

$$s_0 = \frac{EIA}{2rv\rho_s\omega}. \tag{4.23}$$

So far, we have managed to find the relationship between the displacement amplitude, subsequently sound intensity, and the force density amplitude. In order to get an estimate for I_B, first we have to find the relation between bending moment and force density amplitude, but how? The answer is, very easily.

Actually we have already found this relation before. By looking carefully at Eq. (4.20), we can relate M_B and EIA_B. Namely,

$$M_B = D_m(\omega) = d_m(\omega) EIA_B = \frac{(\frac{m\pi}{L})^2}{[(m^4(\frac{\pi}{L})^4 - \frac{\mu}{EI}\omega^2)^2 + (\frac{c_\perp}{EI})^2\omega^2]^{1/2}} EIA_B. \tag{4.24}$$

Substituting the above relation for EIA_B into Eq. (4.23) gives the *minimum required displacement amplitude*, s_{0B}, to break a MT,

$$s_{0B} = \frac{M_B}{2rv\rho_s\omega d_m(\omega)}. \tag{4.25}$$

Finally, using the relation between intensity and pressure amplitude of sound [19], we obtain

$$Intensity = \frac{1}{2}\rho_s v\omega^2 s_0^2. \tag{4.26}$$

We can now find the final formula for the minimum required ultrasound intensity to break a MT as

$$I_B = \frac{1}{2v\rho_s}[\frac{M_B}{2rd_m(\omega)}]^2. \tag{4.27}$$

At this point, we substitute physical values for the parameters in Eq. (4.27) to estimate I_B for a 10 μm length MT inside an aqueous solution. M_B was also estimated at the beginning of this section. Using Fig. 4.6 to evaluate $d_{m(\omega_m)}$ for mode numbers 67, 99 and 149, we find 213 KW/m^2, 363 KW/m^2, and 397 KW/m^2 for I_B, respectively. These intensities correspond to 173.3 dB, 175.6 dB, and 176.0 dB, respectively. These theoretical predictions should be relatively straight-forward to validate experimentally.

4.7 Discussion and Conclusion

Needless to say, achieving resonance is important in order to control the transfer of energy to the MT and to attain its maximum rate. Here, we have shown that the ultrasound plane wave cannot provide the resonance condition for the MT as it excites all the odd number modes at the same time. In order to achieve resonance we should excite only a single mode of the MT. Single mode excitation also helps to noticeably reduce (by 4 orders of magnitude) the total energy transfered to the surrounding medium since it needs a much smaller sound intensity, compared to the multi mode excitation. Another important aspect of the single mode excitation is the fact that the amplitude of the bending moment is almost independent of the mode number. This will help excite a higher mode in order to achieve the resonance condition with a high quality factor and a high amplitude at the same time.

In recent experiments [21] solutions containing assembled and unassembled tubulin were subjected to waves produced by a microwave generator in the range between 0.8 GHz and 2.5 GHz. While the spectrum analyzer detected no significant changes in the case of free tubulin in solution and the control buffer solution with no protein, samples containing microtubules in solution showed a resonance phenomenon centered at 1.51 GHz. This was interpreted as indicating resonant absorption of electromagnetic energy at a frequency range within that predicted in this thesis. The author suggested a mechanical mode of behavior in the case of microtubules, as opposed to free tubulin of buffer solution, a conclusion that is consistent with our conclusions.

Bibliography

[1] J. E. Kennedy, G. R. ter Haar, and D. Cranston, British Journal of Radiology 76, 590-599 (2003).

[2] F. Wu, Z. Wang, H. Zhu, W. Chen, J. Bai, K. Li, C. Jin, F. Xie, and H. Su, Radiology 236, 1034-1040 (2005).

[3] M. W. Miller, D. L. Miller, A. A. Brayman, Ultrasound in Medicine and Biology 22, 9, 1131-1154 (1996).

[4] I. Hrazdira, J. Skorpikova, M. Dolnikova, European Journal of Ultrasound 8, 43-49 (1998).

[5] A. Spadoni and C. Daraio, PNAS 107, 7230-7234 (2010).

[6] S. S. Rao, Mechanical Vibration, 4th ed., Pearson Prentice Hall, Upper Saddle River, New Jersey (2004).

[7] J. M. Gere and S. P. Timoshenko, Mechanics of Materials, 3rd SI ed., Chapman & Hall, London (1991).

[8] K. T. McDonald, Am. J. Phys. 68, 486-488 (2000).

[9] K. C. Neuman and S. M. Block, Rev. Sci. Instrum. 75, 2787-2809 (2004).

[10] J. B. Marion, Classical Dynamics of Particles and Systems, 2nd ed., Academic Press Inc., New York, New York (1970).

[11] G. B. Arfken and H. J. Weber, Mathematical Methods for Physicists, 5th ed., Harcourt/Academic Press, San Diego, California (2001).

[12] L. A. Segel, Mathematics Applied to Continuum Mechanics, Dover Publications Inc., New York (1987).

[13] J. Howard, Mechanics of Motor Proteins and the Cytoskeleton, Sinauer Associates Inc., Sunderland, Massachusetts (2001).

[14] M. Kikumoto, M. Kurachi, V. Tosa, and H. Tashiro, Biophysical Journal 90, 1687-1696 (2006).

[15] M. Kurachi, M. Hoshi, and H. Tashiro, Cell Motil. Cytoskeleton 30, 221-228 (1995).

[16] A. Samarbakhsh and J. A. Tuszynski, Phys Rev. E 80, 011903 (2009).

[17] D. J. Odde, L. Ma, A. H. Briggs, A. Demarco, and M. W. Kirschner, J. Cell Sci. 112, 3283-3288 (1999).

[18] C. M. Waterman-Storer and E. D. Salmon, J. Cell Biol. 139, 417-434 (1997).

[19] D. Halliday, R. Resnick, J. Walker, Fundamental of Physics, 6 ed., John Wiley & Sons Inc., New York, New York (2000).

[20] L. E. Kinsler, A. R. Frey, A. B. Coppens, and J. V. Sanders, Fundamentals of Acoustics, 4th ed., John Wiley & Sons Inc., New York, New York (2001).

[21] R. Pizzi, G. Strini, S. Fiorentini, V. Pappalardo, M. Pregnolato, A chapter of the following book: "Artificial Neural Networks", Nova Publishers, New York (To be published).

Chapter 5

General Discussion and Conclusions

5.1 Summary

The shooting bead method introduced in this thesis can be performed very fast and has numerous advantages over the other current methods for finding the exural rigidity of the bio- and nano-laments.

For performing this experiment, the bead needs not be attached to the filament (like the buckling force method [1, 2]), in fact, this was one of the reasons that guided the introduction of the proposed method. It needs just a single trap (the buckling force method needs two traps), there is no need to find the force exerted on the bead by the trap (which is very sensitive measurement), there is no need to know the exact shape of the filament (which is required for the buckling force and the thermodynamic fluctuation methods [3]), there is no need to oscillate the trap (like in the wiggle method [4]),

there is no need to measure the time (as in the relaxation method [5]), and there is no need to measure the velocity of the bead or the rod (as in the hydrodynamic flow method [6, 7]). The only measurement that we need to perform is the measurement of the length for a and d, also because the ratio of a/d is important not a and d individually, there is no need to calibrate the microscope. Most importantly, from the author's point of view, this method provides a compact parametric formula for the flexural rigidity (most of the above methods lack this advantage so that even after several measurements still there is need for some theoretical work to be done in order to find the flexural rigidity) which helps to calculate the flexural rigidity or any other unknown in the formula after a single easy measurement. Also, knowing the cross-section of the filament exactly and measuring the flexural rigidity, we are able to calculate the Young modulus of the filament

In extension of the method, for consideration of the effects of the energy loss due to the filament itself on the calculated value for the flexural rigidity, we could define a new parameter (the filament drag factor) which is responsible for the all contributions of the viscous force on the filament. With finding a new parametric formula, we could prove that the effects of filament energy loss are more important when dealing with filaments with less rigidity. Also beautifully this new formula for the flexural rigidity converts to the old formula, when we ignore the effects of the filaments drag force by changing the filament drag factor to one.

In the last project, our goal was to determine conditions for the resonance condition of the microtubule when it is under the influence of mechanical (usually ultrasound) waves. Achieving resonance is important in order to control the transfer of energy to the MT and to attain its maximum rate.

As microtubules are the major filaments of the cytoskeleton and they are directly involved in the process of mitosis during the cell division, possible breakage of a microtubule during mitosis can control the duplication of cancer cell (as cancer cells duplicate more rapidly than the normal cells and they spend more percentage of their lifetime in the mitosis stage). Here, we have shown that the ultrasound plane wave cannot provide the resonance condition for the MT as it excites all the odd number modes at the same time. We have also shown that, in order to achieve resonance we should excite only a single mode of the MT but the single mode number of this mode should be larger than a minimum mode number. A parametric analytical relation for this minimum mode number has been introduced in this thesis. Single mode excitation also helps to noticeably reduce (by 4 orders of magnitude) the total energy transfered to the surrounding medium since it needs a much smaller sound intensity, compared to the multi-mode excitation and it helps to transfer the minimum amount of energy to other organs. Another important aspect of the single mode excitation is the fact that the amplitude of the bending moment is almost independent of the mode number . This will help excite a higher mode in order to achieve the resonance condition with a high quality factor and a high amplitude at the same time. Our theoretical results for the range of resonance frequency are completely in agreement with the new experimental data. The most satisfying aspect of carrying out this project (which from the authors point of view is the definition of theoretical physics) is the fact that our theoretical work has been done a few months before the experiment performed which is usually the other way around these days.

It is worth pointing out that in a recent paper [8], other authors have used our analytical method for consideration of the effect of viscosity on the

filament, to correct the viscous drag induced error in macromolecular manipulation experiments using atomic force microscope.

5.2 Motivation and Preliminary Experimental Work

Figure 5.1 shows two images of a single bio-filament that has been produced due to the aggregation of the tubulin protein in the laboratory [9] under two different experimental situations. The image in the top panel shows a trapped bead in a laser tweezer which has pushed the filament in the south-east direction. To convince the reader that the bead is pushing on the filament, we should bring to the reader's attention the slope of the angle between the filament (although the filament is not completely straight in this situation) and the horizontal line in the two states. In the bottom image the bead is not in the laser trap anymore and has been pushed by the filament in the north-west direction where it has reached its final position. Seeing this effect of a "jumping bead" in the lab was our main motivation to find a final relation for one of the important characteristics of the bio-filaments and nano-filaments just with very fast and easy measurement of the initial and final position of the bead. Actually we had planned to do a different measurement. Unfortunately that experiment was a failure and the bead didn't attach to the filament but suddenly this jumping effect happened and its observation led to the development of the shooting bead method.

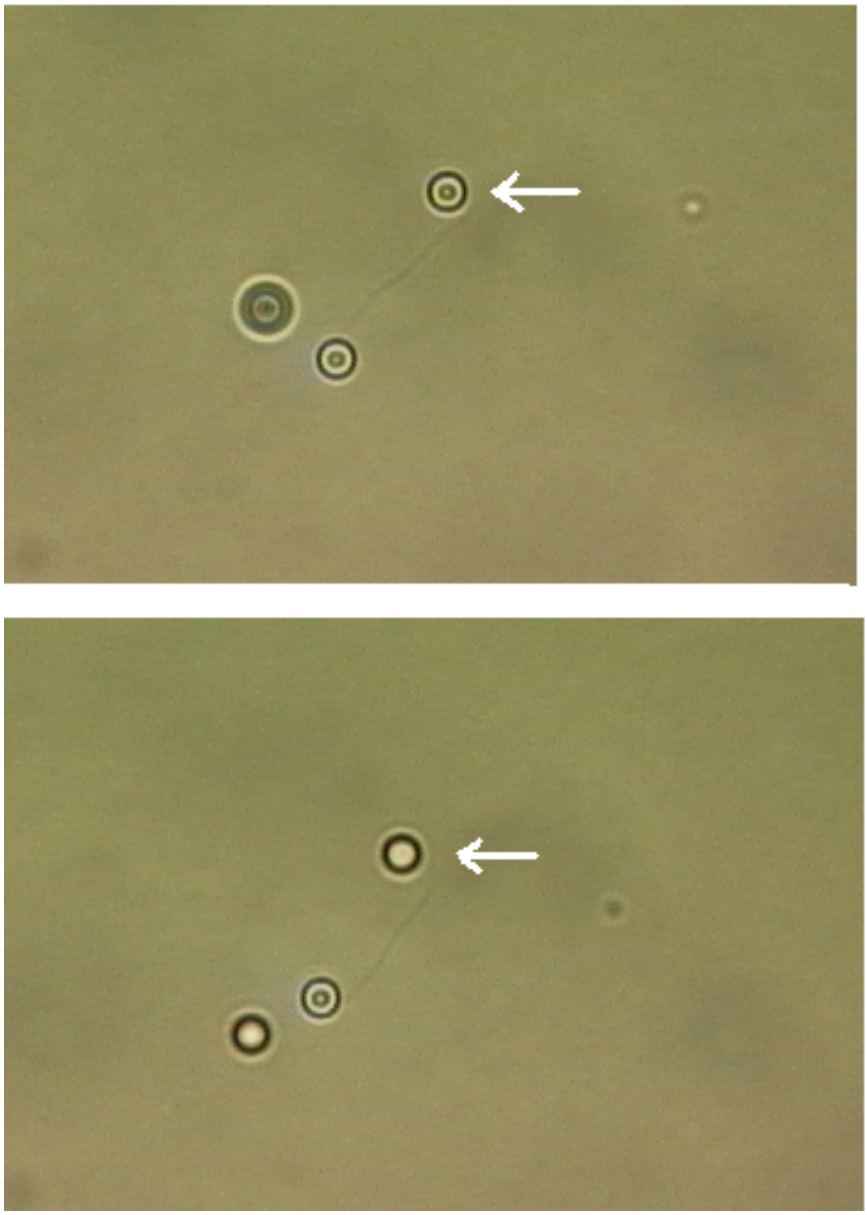

Figure 5.1 Two pictures of a bio-filament in two different situations. The top panel shows a trapped bead in a laser tweezer which has pushed the filament in the south-east direction. The bottom panel shows that the bead is not in the laser trap anymore and has been pushed by the filament in the north-west direction and has reached its final position. The radius of the beads is roughly 1 μm. Picture taken by Dr. Linda Payet.

5.3 Future Works

At the beginning of my studies on this project, I spent more than a year working on the development of a physical model for the conformation of a microtubule from tubulin dimers based on the electrostatic forces. Most of the available models on this subject are not based on direct force and they just use other ideas like the random walk model. I discuss the idea very briefly below:

It is known that tubulin dimer has a dipole moment, $\mathbf{p}$, [10–13] which is not aligned with the axes of tubulin dimer [14] (axes of a tubulin dimer is aligned with the protofilament when the tubulin is contributed in the microtubule). As a microtubule is also made from tubulin dimers (Figure 5.2), it produces a nonuniform electric field, $\mathbf{E}$, in the cytoplasm. The force exerted on a free tubulin dimer due to a microtubule can be calculated from the following formula:

$$\mathbf{F} = (\mathbf{p}.\nabla)\mathbf{E}. \tag{5.1}$$

There will be also a torque exerted on the free tubulin. This torque just aligns the tubulin with the electric field line due to the microtubule. As a result we just need to calculate the exerted force on the tubulin dimer when its dipole moment aligned with electric field line. This fact reduces the complexity of the calculations extensively. With calculating this force and using the fact that this force is proportional to the velocity of the free tubulin dimer through the Stokes' law and integrating over the surface which has surrounded the microtubules cap, we can find an estimation for the growth rate of microtubule.

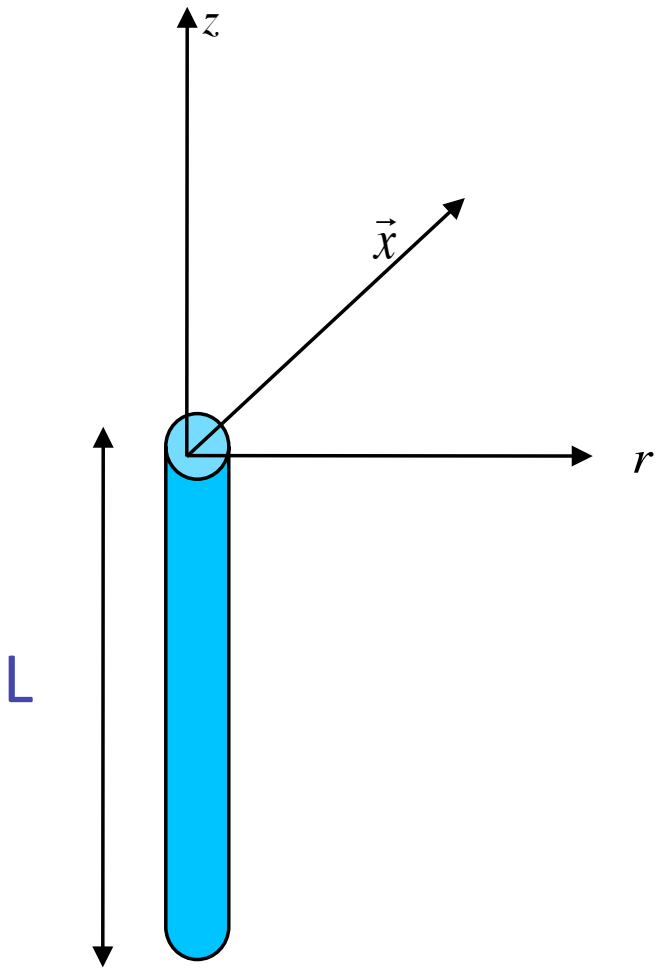

Figure 5.2 Schematic diagram of microtubul made of electric dipoles which produces electric field in the cytoplasm.

This work will be continued in the future.

Another project which I was working on, is calculating the assembled energy of the MT and tubulin sheet. In this project we want to answer important questions about the process of folding tubulin sheets to form MT cylinders (this is based on the hypothesis proposed by M-F Carlier and A. Pantaloni that the MTs acquire their tubular shape from a sheet) and also giving a necessary condition for the electric dipole direction of a single tubulin dimer. To answer these questions I have written 2 computer codes (and still have to write 2 more codes) that calculate the assembled energy of the two cases, tubular form and the sheet. Comparing these four figures reveals whether this folding effect is possible or not (I strongly tend to believe that this is not possible). Also we will be able to find a subset of values for the direction of the electric dipole moment of a tubulin dimer. I briefly discuss the method below.

Dipole- dipole interaction energy can be calculated from the following equation:

$$U = \frac{\mathbf{P}_1.\mathbf{P}_2 - 3(\mathbf{n}.\mathbf{P}_1)(\mathbf{n}.\mathbf{P}_2)}{4\pi\epsilon_0 r^3} = -\frac{P_1 P_2}{4\pi\epsilon_0 r^3}(2\cos\theta_1\cos\theta_2 - \sin\theta_1\sin\theta_2\cos\psi). \tag{5.2}$$

where $\mathbf{P}_1$ and $\mathbf{P}_2$ are two points dipole moments, r is the distance between the two dipoles, $\mathbf{n}$ is the unit vector pointig toward one dipole from the other one, θ_1 and θ_2 are the angle between the first dipole and second dipole with respect to $\mathbf{n}$ respectively. ψ is the angles between projections of $\mathbf{P}_1$ and $\mathbf{P}_2$ on the plane perpendicular to $\mathbf{n}$. Figure 5.3 shows the schematic diagram of orientation of two dipoles.

Now, to calculate the interaction energy for a MT consisting of $m \times n$

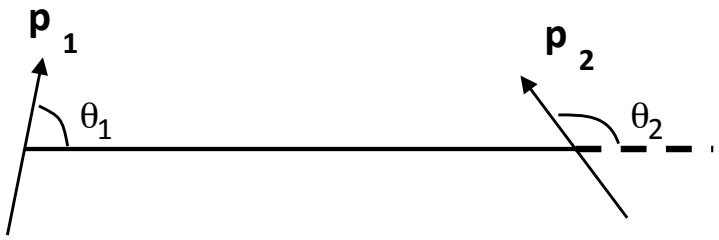

Figure 5.3 Schematic diagram of orientation of two dipoles.

tubulin dimers (n is the number of protofilaments and m is the number of tubulin units in each protofilament (Figure 5.4), we have to calculate $[m \times n \times (m \times n - 1)/2]$ of such dipole-dipole interaction potential terms and add them together for any direction in 3D space. Comparing the result (2D graphs) we can find an answer of our question. This work also will be continued in the future.

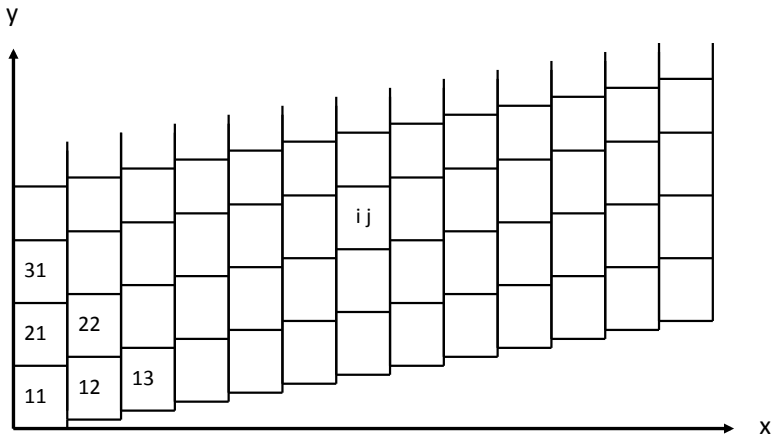

Figure 5.4 Consideration of microtubule as a $m \times n$ matrix.

Bibliography

[1] M. Kikumoto, M. Kurachi, V. Tosa, and H. Tashiro, Biophysical Journal 90, 1687-1696 (2006).

[2] M. Kurachi, M. Hoshi, and H. Tashiro, Cell Motil. Cytoskeleton 30, 221-228 (1995).

[3] F. Gittes, B. Mickey, J. Nettleton, and J. Howard, J. Cell Biol. 120, 923-934 (1993).

[4] H. Felgner, R. Frank, and M. Schliwa, J. Cell Sci. 109, 509-516 (1996).

[5] H. Felgner, R. Frank, J. Biernat, E.-M. Mandelkow, E. Mandelkow, B. Ludin, A. Matus, and M. Schliwa, J. Cell Biol. 138, 1067-1075 (1997).

[6] P. Venier, A. C. Maggs, M.-F. Carlier, and D. Pantaloni, J. Biol. Chem. 269, 13353-13360 (1994).

[7] J. C. Kurz, and R. C. Williams, Jr., Biochemistry 34, 13374-13380 (1995).

[8] R. Liu, M. Roman, and G. Yang, Rev. Sci. Instrum. 8, 063703 (2010).

[9] The experiment is done by Dr. Linda Payet.

[10] R. Stracke, K. J. Bohm, L. Wollweber, J. A. Tuszynski, and E. Unger, Bioch. Biophys. Res. Commun. 293, 602609 (2002).

[11] J. A. Tuszynski, S. Hameroff, M.V. Sataric, B. Trpisova, and M. L. A. Nip, J. Theor. Biol. 174, 371380, (1995).

[12] A. Brown, PhD Thesis, University of Alberta, Edmonton, Canada, (1999).

[13] M. V. Sataric, J. A. Tuszynski, and R. B. Zakula, Phys. Rev. E 48(1), 589597 (1993).

[14] S. Hagan, S. R. Hameroof, and J. A. Tuszynski, Phys. Rev. E 65, 061901 (1998).

[15] J. E. Schoutens, J. Biol. Phys. 31, 35-55, (2005).

Appendix A

Calculating the Order of Magnitudes for Vertical Displacement Due to the Buoyant Force and the Weight of the Bead

It has been assumed that the density of the bead is equal or close to the density of the solution (in most cases this will be composed mainly of water) which means that the buoyant force and the weight of the bead cancel each other out. Therefore, we need not make a correction for the apparent weight of the bead but this method still works even if the density of the bead is different from the density of the solution because of the following two reasons. Referring to Figure 3.1 which is in a horizontal plane, the vertical forces (the effects of gravity and buoyant forces) do not provide any contribution to the horizon-

tal motion. Secondly, the experiment pertains to a process that occurs in a fraction of a second which depends on an asymptotic approach time constant. In this appendix we estimate how much the bead moves vertically during the experiment assuming the density of the bead is different from the density of the solution. If this distance, b, is large with respect to the length of the focal region of the microscope, the resolution of the image of the bead after the experiment will be lost.

The vertical force exerted on the bead is $|m - m_s|g$ where m_s denotes the displaced mass of the solution. Therefore, the vertical acceleration of the bead is

$$a_z = \frac{m - m_s}{m} g. \tag{A.1}$$

The elapsed time for this motion is on the order of the asymptotic approach time constant, therefore the total vertical distance is on the order of $g(m - m_s)(9\tau)^2/2m$ or

$$b \sim O(\frac{9}{8} mg \frac{|m - m_s|}{\pi^2 \eta^2 R^2}). \tag{A.2}$$

With a typical value of η=10 $^{-3}$ Pa.s for water, R=1 μm, m_s=$\frac{1}{2}m \simeq 4 \times 10^{-15}$ kg for aqueous solution, we obtain $b \sim O(10^{-13})$m.

This means that the vertical displacement due to the buoyant force and the weight of the bead during the experiment is definitely negligible and we will not lose the focus when viewing the bead after it stops.

Appendix B

Energy Conservation Investigation

It is important to validate the solution by making sure that the initial potential energy of the filament is equal to the total energy-loss (Q) of the bead due to the viscous drug force exerted on it over the course of its motion. Infinitesimal energy-loss of the bead during its motion is given by

$$dQ = -dW_v = -F_v dx = 6\pi\eta R\dot{x}^2 dt. \tag{B.1}$$

Note that in the above equation we calculate the negative of the work done on the bead by the viscous drag force in order to arrive at a positive value for the energy-loss of the system. The value of $\dot{x}^2$ can be found by taking the derivative of Equation (3.2) and squaring it, so that

$$\dot{x}^2 = a^2 \exp(-2\Lambda t)\,(\Lambda^2 \cos^2 \Omega t + \Omega^2 \sin^2 \Omega t + \Lambda\Omega \sin 2\Omega t). \tag{B.2}$$

From Equations (B.1) and (B.2) we obtain

$$Q_1 = 3\pi\eta R a^2 \int_0^{t_0} \exp\left(-2\Lambda t\right)\left(\Lambda^2 + \Omega^2 + (\Lambda^2 - \Omega^2)\cos 2\Omega t + 2\Lambda\Omega \sin 2\Omega t\right)\, dt. \tag{B.3}$$

The subscript 1 in Q_1 indicates that this is energy-loss that occurred in the first part of the motion (underdamped harmonic motion from $t = 0$ to $t = t_0 = \pi/2\Omega$). The result of the above equation is

$$Q_1 = \frac{1}{2}ka^2 - \frac{1}{2}ma^2\Omega^2 \exp(-\frac{\Lambda}{\Omega}\pi). \tag{B.4}$$

Energy-loss in the second part of the motion (damped motion) can be found using the following integral:

$$Q_2 = 6\pi\eta R \int_0^{\infty} a^2\Omega^2 \exp(-\frac{\Lambda}{\Omega}\pi)\exp(-4\Lambda t)dt = \frac{1}{2}\frac{3\pi\eta R}{\Lambda}a^2\Omega^2 \exp(-\frac{\Lambda}{\Omega}\pi). \tag{B.5}$$

From Equation (B.4) and (B.5) we find that the total energy-loss of the bead during its whole motion is exactly equal to the potential energy stored in the filament just before releasing the bead. This then validates the solutions we found earlier in the paper.

Although to prove the conservation of energy we did not need to calculate the bead energy-loss in terms of measurable quantities a and d, for completeness of the solution we evaluate Q_1 in terms of those quantities. In order to do that we have to replace k and Ω in Equation (B.4) in terms of a and d. Note that k in terms of a and d has been already found in Equation (3.4) and inserting this equation into Equation (3.5) we easily find the following equations for k and Ω:

$$k = m\Lambda^2 \left(\frac{\pi^2}{4[W\left(\frac{\pi a}{4d}\right)]^2} + 1 \right), \quad \Omega = \frac{\pi\Lambda}{2W(\frac{\pi a}{4d})}. \tag{B.6}$$

Replacing the above expressions in Equation (B.4) followed by some simple algebra gives

$$Q_1 = \frac{1}{2} m a^2 \Lambda^2 (\frac{\pi^2}{4[W(\frac{\pi a}{4d})]^2}(1 - \exp(-2W(\frac{\pi a}{4d}))) + 1). \tag{B.7}$$

Appendix C

Calculating the Ratio of the Rod's Swept Area to the Filament Swept Area

Under the small-angle approximation, the deflection of a beam, y, with length L as a function of distance with respect to the pivot, x (See Figure3.2), can be easily found by solving the beam equation [29],

$$y(x) = \frac{a}{2L^3}(3Lx^2 - x^3). \tag{C.1}$$

By integrating the above equation from 0 to L, the area swept by the filament (curved AD) is

$$S_{AD} = \frac{3}{8}aL. \tag{C.2}$$

The area swept by the rod (BD) in the case of small deflection is

$$S_{BD} = \frac{1}{4}aL. \tag{C.3}$$

Dividing Equation (C.3) by Equation (C.2) yields the ratio we seek.

Appendix D

Calculation of $\delta\kappa_0$ and $\delta\kappa$

We know that

$$\kappa_0 = \frac{9\pi\eta^2 L^3}{4\rho R}, \tag{D.1}$$

thus for $\delta\kappa_0$ we have

$$\delta\kappa_0 = \kappa_0(\frac{\delta\rho}{\rho} + \frac{2\delta\eta}{\eta} + \frac{\delta R}{R} + \frac{3\delta L}{L}). \tag{D.2}$$

ρ and η can be measured very accurately (as we use the values for the bulk material), a typical value for $\delta R/R$ for a good microsphere is 0.02 and $\delta L/L$ can be considered as 0.01. It means the percentage error for $\delta\kappa_0$ can be almost 5%.

Finding $\delta\kappa$ with the knowledge of $\delta(\kappa/\kappa_0)$ from Equation (3.23) and $\delta\kappa_0$ from Equation (D.2) is now straightforward,

$$\delta\kappa = \delta(\frac{\kappa}{\kappa_0})\kappa_0 + \frac{\kappa}{\kappa_0}\delta\kappa_0. \tag{D.3}$$

Appendix E

Coefficient of Expansion in Eq. (4.13)

Here we want to calculate the coefficients of the Fourier sine series for the following function in the interval]-L, L[

$$f(x) = \begin{cases} -1 & -L < x < 0 \\ 0 & x = 0 \\ 1 & 0 < x < L \end{cases} \tag{E.1}$$

Coefficients of cosine terms will be

$$a_n = \frac{1}{L}(-\int_{-L}^{0} \cos(\frac{n\pi s}{L})ds + \int_{0}^{L} \cos(\frac{n\pi s}{L})ds) = 0. \tag{E.2}$$

It was obvious as the above function is an odd function.

Also the coefficients of sine terms will be

$$b_n = \frac{1}{L}(-\int_{-L}^{0} \sin(\frac{n\pi s}{L})ds + \int_{0}^{L} \sin(\frac{n\pi s}{L})ds) = \begin{cases} 4/n\pi & n \text{ is an odd number} \\ 0 & n \text{ is an even number} \end{cases} \tag{E.3}$$

Using above equations we obtain

$4\pi[\sin(\pi x/L)/1 + \sin(3\pi x/L)/3 + \sin(5\pi x/L)/5 + ...] = 1$ for $0 < x < L$.